Journal of Experimental Botany, Vol. 58, No. 4, pp. 881–898, 2007
Imaging Stress Responses in Plants Special Issue
doi:10.1093/jxb/erl142 Advance Access publication 9 October, 2006

Journal of Experimental Botany

SPECIAL ISSUE PAPER

3D lidar imaging for detecting and understanding plant responses and canopy structure

Kenji Omasa*, Fumiki Hosoi and Atsumi Konishi

Graduate School of Agricultural and Life Sciences, The University of Tokyo, Yayoi 1-1-1, Bunkyo-ku, Tokyo, 113-8657 Japan

Received 5 May 2006; Accepted 24 July 2006

Abstract

Understanding and diagnosing plant responses to stress will benefit greatly from three-dimensional (3D) measurement and analysis of plant properties because plant responses are strongly related to their 3D structures. Light detection and ranging (lidar) has recently emerged as a powerful tool for direct 3D measurement of plant structure. Here the use of 3D lidar imaging to estimate plant properties such as canopy height, canopy structure, carbon stock, and species is demonstrated, and plant growth and shape responses are assessed by reviewing the development of lidar systems and their applications from the leaf level to canopy remote sensing. In addition, the recent creation of accurate 3D lidar images combined with natural colour, chlorophyll fluorescence, photochemical reflectance index, and leaf temperature images is demonstrated, thereby providing information on responses of pigments, photosynthesis, transpiration, stomatal opening, and shape to environmental stresses; these data can be integrated with 3D images of the plants using computer graphics techniques. Future lidar applications that provide more accurate dynamic estimation of various plant properties should improve our understanding of plant responses to stress and of interactions between plants and their environment. Moreover, combining 3D lidar with other passive and active imaging techniques will potentially improve the accuracy of airborne and satellite remote sensing, and make it possible to analyse 3D information on ecophysiological responses and levels of various substances in agricultural and ecological applications and in observations of the global biosphere.

Key words: Carbon stock, canopy structure, chlorophyll fluorescence, leaf temperature, lidar, photosynthesis, plant growth, stomatal response, three-dimensional (3D) imaging, remote sensing.

Introduction

Passive and active imaging techniques have come into widespread use for plant analysis at the subcellular level, the whole-plant level, and the ecosystem and remote-sensing levels (Mayers, 1983; Hashimoto *et al*., 1990; Hobbs and Mooney, 1990; Omasa, 1990, 2006; Häder, 1992, 2000; Lichtenthaler *et al*., 1996; Ustin *et al*., 1999; Buschmann *et al*., 2000; Govindjee and Nedbal, 2000; Lefsky *et al*., 2002*b*; Omasa *et al*., 2002*a*, 2005, 2006; Jones, 2004; Oxborough, 2004; Papageorgiou and Govindjee, 2004; Zarco-Tejada *et al*., 2004; Chaerle *et al*., 2005; Kolber *et al*., 2005; Schurr *et al*., 2006). One recent trend in imaging techniques is the adoption of three-dimensional (3D) imaging.

The 3D structure of leaves and plants plays an important role in sustaining plant functions such as photosynthesis and transpiration and in determining the suitability of different habitats for various species. Therefore, it is necessary to obtain 3D information to improve understanding of plant functioning and habitats. The 3D information can also serve as a good indicator of plant stress and improve understanding of stress responses. For example, stresses such as a water

* To whom correspondence should be addressed. E-mail: aomasa@mail.ecc.u-tokyo.ac.jp
Abbreviations: CHP, canopy height profile; DBH, diameter at breast height; DCHM, digital canopy-height model; DEM, digital elevation model; DTM, digital terrain model; FP-mode, first-pulse mode; GPP, gross primary production; GPS, global positioning system; IMU, internal measurement unit; InSAR, interferometric synthetic-aperture radar; LAD, leaf area density; LAI, leaf area index; lidar, light detection and ranging; LIF, laser-induced fluorescence; LIFT, laser-induced fluorescence transient; LP-mode, last-pulse mode; NPP, net primary production; PPFD, photosynthetic photon flux density; PRI, photochemical reflectance index; RMSE, root-mean-square error; SAR, synthetic-aperture radar; VCP, voxel-based canopy profiling.

deficit and severe heat can change the shape and morphology of individual plants. On a large scale, environmental changes can induce extensive plant responses, such as changes in forest growth, species composition and global carbon cycling. These responses also involve changes in the 3D structure of plants and vegetation canopies. Therefore, 3D plant analysis is indispensable for understanding responses of ecosystems and individual plants.

Methods for 3D imaging are divided broadly into two types: passive and active. Passive methods include stereovision and shape-from-*x* (where *x* represents focus, shading, texture, contour, and other parameters) algorithms. In particular, stereovision has been used in a wide range of scientific research and industrial applications. It allows 3D reconstruction of an object based on the use of geometrical rules of perspective and based on the difference between two or more images of objects taken from different positions. Although some studies have reported the application of stereovision with small plants (He *et al*., 2003; Andersen *et al*., 2005) and field crops (Ivanov *et al*., 1994, 1995), plants are a difficult target for stereovision because they have complex structures; leaves have a range of shapes and textures, and create discontinuities (i.e. they may hide each other). Mismatches between the corresponding points in different images (the so-called 'correspondence problem') and self-occlusion within an object remain major problems in stereovision, and increase with increasing complexity of plant shape. Dynamic stereo is another trend in stereovision, in which motion is used to provide a more reliable 3D reconstruction (Negahdaripour *et al*., 1995; Brooks *et al*., 1998). In one example of this approach, Schurr *et al.* (2001) employed a single camera that they moved continuously from one stereo position to another. They simplified the correspondence problem by tracking each pixel throughout the acquired image sequence and used this improved information to calculate the 3D position of the leaf surface. However, it is difficult to handle the large amount of data from multiple frames generated by this technique. Airborne or satellite-based stereoscopic methods have been widely used for large-scale terrestrial and forest observations (Gong *et al*., 2002; Zomer *et al*., 2002; Hay *et al*., 2004; Eckert *et al*., 2005). Although their accuracy has been improved by using sensors with high spatial resolution (Sheng *et al*., 2001; Toutin, 2004), the resolution and accuracy (several metres) remain insufficient for obtaining detailed 3D information for vegetation. In addition, image quality is affected by sunlight and weather conditions. Shape-from-*x* algorithms are not commonly used compared with stereovision because of limitations in the technique. For example, a shape-from-focus algorithm proved to be suitable for use with a light microscope, but was limited to use at short distances (within 20–30 m) with a 3D camera (Omasa, 2000, 2006). The use of such passive methods is limited to objects with clearly defined and fine-grained texture.

Active methods are not limited to specific surface textures because they are designed to generate wavelengths of electromagnetic radiation (rather than relying on reflected or emitted ambient radiation) that are suitable for the specific type of 3D measurement. Synthetic-aperture radar (SAR) is a form of active sensor that allows measurement of the physical characteristics of the ground surface using microwaves during all weather conditions, as well as during the day and night. In particular, interferometric synthetic-aperture radar (InSAR) has been applied for determining the height of vegetation canopies (Hagberg *et al*., 1995; Askne *et al*., 1997; Papathanassiou and Cloude, 2001; Kellndorfer *et al*., 2004). InSAR can estimate ground elevations based on phase differences in images acquired from different locations. However, the complexity of the scattering process within vegetation makes it difficult to separate physical forest parameters based on the interferometric data (Papathanassiou and Cloude, 2001). Furthermore, the method is useful for large-scale observation, but its accuracy is of the order of several metres and is thus insufficient to provide a detailed description of the 3D structure of plants.

Recently, light detection and ranging (lidar) using laser scanners has emerged as a powerful active sensing tool for direct 3D measurement of plant shapes and canopy structures. Lidar can obtain accurate 3D information for plants by measuring the distance between the sensor and a target. The scales of application have ranged from small plants to forest stands. Numerous studies have shown the usefulness of lidar for the estimation of 3D plant properties (Næsset, 1997; Means *et al.*, 1999; Omasa *et al*., 2000, 2002*b*; Hyyppä *et al*., 2001; Lefsky *et al*., 2002*b*; Næsset *et al*., 2004; Yu *et al*., 2004; Reutebuch *et al*., 2005). However, the potential of lidar has not yet been fully exploited for monitoring plant responses to stress.

In the present paper, recent research on lidar imaging is reviewed, including aerial remote sensing for 3D measurements of plant shape and canopy structure, and then the potential of lidar for monitoring plant responses to stress is described. A demonstration is also provided of the potential of composite imaging that combines lidar data with data provided by other imaging techniques.

Development of lidar systems

Lidar is also called a 'laser radar', 'laser scanner', 'laser profiler', 'range finder', or 'laser ranger'. Recently, it has been used as a novel active sensing tool for 3D measurement of plant shapes and canopy structures. Lidar can accurately measure the distance between the sensor and a target based on the elapsed time between the emission and return of laser pulses (the 'time of flight' method) or based on trigonometry (the 'optical probe' or 'light section' methods). The accuracies of airborne and ground-based lidar systems are typically ~0.1–1 m and ~0.05–10 cm,

respectively, so lidar can replace conventional passive methods for 3D measurement. Lidar systems are divided into several categories according to their characteristics.

Early studies of non-scanning airborne lidar systems

Airborne lidar systems were initially developed for bathymetric work (Hickman and Hogg, 1969; Hoge *et al*., 1980). In the 1980s, lidar systems were applied in topographic mapping. Krabill *et al.* (1984) used an airborne lidar system to map the topography of a watershed near Memphis, Tennessee. Schreier *et al.* (1984) determined, in a terrain mapping study in Canada, that 95% of all laser terrain elevations were within 1.8 m of photogrammetrically derived values. In this application, vegetation was regarded as an obstruction and a source of noise when terrain elevations were calculated based on laser profiles. After the mid-1980s, lidar was also used for the determination of vegetation canopy heights. Nelson *et al*. (1984) utilized lidar on a heavily forested hardwood site in Pennsylvania to show that changes in the laser canopy profile corresponded to changes in canopy density. They found that the mean tree height estimates were within 60 cm of the photogrammetric values, but that the laser estimates were more precise. Some biophysical properties of forests, such as gross merchantable timber volume and biomass, have been estimated from lidar-derived tree heights (Maclean and Krabill, 1986; Nelson *et al*., 1988). These experiments showed that lidar can be a useful tool for estimating forest properties.

Airborne small-footprint scanning lidar systems

Lidar systems in the 1980s were non-scanning types, and only a single line of data directly beneath the aircraft could be obtained as a cross-sectional profile. The systems thus had limitations for covering wide areas. In the mid-1990s, airborne-scanning lidar became available and this technology was applied for topographic terrain mapping and forest measurements (Flood and Gutelius, 1997; Næsset, 1997; Hyyppä and Inkinen, 1999; Omasa *et al*., 2000). Scanning systems can sweep a swath of terrain by means of lateral deflection of the emitted laser beams during forward movement of the aircraft. Consequently, a large area can be scanned as a series of swaths. The footprint diameter (i.e. the diameter of the laser beam on the ground) is relatively small, typically ~10–30 cm. The position of the laser beam on the ground can be determined with an absolute accuracy of ⩽0.5 m and a relative accuracy of 0.15 m (Omasa *et al*., 2000) by recording the movements of an aircraft and its lidar instrument using ground-based and aerial global positioning system (GPS) receivers and an aerial internal measurement unit (IMU). The range resolution and accuracy of the lidar system are within 1 cm and 15 cm, respectively. The lidar system functions as a discrete-return recording device, since it only receives a single return signal or a small number of return signals from the ground. Figure 1 shows a schematic diagram of 3D measurement using a lidar system. The illustrated helicopter-borne lidar system has two receiving modes (Fig. 1A): a first-pulse mode (FP-mode), in which the first returned pulses are received, and a last-pulse mode (LP-mode), in which the last returned pulses are received.

In the 1990s, the density of laser pulses provided by ordinary small-footprint airborne scanning lidar systems was less than several pulses m^{-2} on the ground, with a pulse repetition frequency of 1–25 kHz. Recent advances in lidar technology have increased this value to >10 pulses m^{-2} with a pulse repetition frequency of up to 100 kHz. Moreover, the density can be increased several-fold using slower flight speeds (e.g. using helicopters rather than airplanes to carry the scanning lidar). These systems can provide high-resolution images of individual trees. Several studies have shown the ability of lidar systems to provide measurements of individual trees (Hyyppä and Inkinen, 1999; Omasa *et al*., 2000, 2003; Hyyppä *et al*., 2001; Brandtberg *et al*., 2003; Holmgren and Persson, 2004; Næsset *et al*., 2004; Yu *et al*., 2004; Reutebuch *et al*., 2005).

Airborne large-footprint scanning lidar systems

Airborne lidars with a large footprint and a large scan width have been developed for a target of forest remote sensing on large scales and from satellites (Blair *et al*., 1999; Lefsky *et al*., 1999*b*, 2002*b*; Means *et al*., 1999; Drake *et al*., 2002). These systems scan with a large footprint, typically ~10–25 m in diameter, and are obtained from a higher altitude, resulting in more complete sampling of the canopy and a wider image swath. The system includes a waveform-recording device that digitizes the power level of the entire return laser signal and captures both the vertical distribution of the backscatter of laser illumination from all canopy elements (both foliar and woody) and reflection from the ground. The range resolution and accuracy are both ~10 cm (Blair and Hofton, 1999). The position of the laser beam on the ground can be determined to within 5–10 m (Means *et al.*, 1999).

Ground-based non-scanning lidar systems

Liu (1995) described an example of a non-scanning ground-based lidar system. The system has a laser source and detector for measuring distances, a compass for measuring azimuth angles, and a tilt sensor for measuring zenith angles. From these measurements, the position of a target is calculated as orthogonal coordinates. Distance is measured using the time-of-flight method, and ranging accuracy is ~10 cm. The system is portable, so a major use of the system (and of comparable non-scanning lidar systems) is for forest surveys, such as traverses of forest stands, stem mapping, and dendrometry (Liu, 1995;

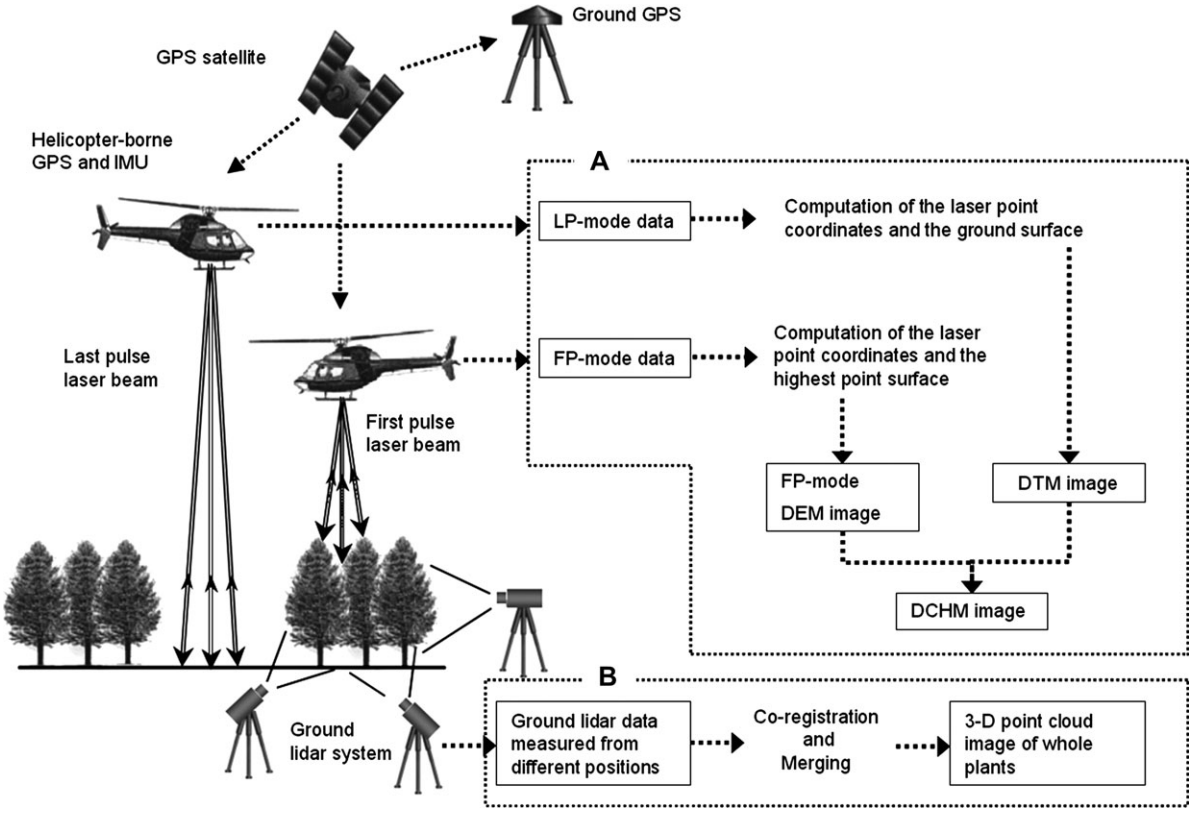

Fig. 1. A schematic diagram of 3D remote sensing using helicopter-borne and ground-based scanning lidar systems. (A) Data processing in a helicopter-borne scanning lidar system. (B) Data processing in a ground-based scanning lidar system. FP-mode, first-pulse mode; LP-mode, last-pulse mode; DEM, digital elevation model; DTM, digital terrain model; DCHM, digital canopy-height model.

Peet *et al*., 1997; Williams *et al*., 1999). Another use involves measurements of vertical foliage profiles using a ground-based lidar system with the beam direction set vertically and the operator manually repositioning the lidar head by walking through the forest (Radtke and Bolstad, 2001; Parker *et al*., 2004).

Ground-based scanning lidar systems

In ground-based scanning lidar systems, rotating or oscillating mirrors within the lidar head or built-in stepping motors automate the horizontal and vertical scanning. These systems can record the configuration of whole plants and foliage structures as a 3D 'point-cloud image' by merging lidar data measured from different positions (Fig. 1B). In stand-scale measurement from a distance >10 m, the time-of-flight method is most often available, and provides a ranging accuracy of ~1 cm (Omasa *et al*., 2002*b*; Urano and Omasa, 2003). However, the ranging accuracy is insufficient to capture foliage and leaf shapes precisely. The phase-shift detection method (Vanderbilt, 1985) and the optical-probe method (Shirai, 1972) are more suitable for precise measurements from <10 m. In the former method, the system modulates the amplitude of the laser beam and converts the difference in the phases of the modulation in the sent and received laser beams into a distance value. In the latter method, a laser beam is projected on an object to create a small spot, and the beam is detected by a photo-detector placed at a certain distance from the laser source but outside the line connecting the laser source and target. The laser spot, laser source, and detector thus form a triangle, and the distance to the object can be calculated by means of trigonometry. For example, one system that uses the optical-probe method can measure foliage and leaf shapes with range accuracies of 0.5 mm at a distance of 3.5 m, and 5 mm at a distance of 10 m under sunlight using a near-infrared laser with a wavelength of 785 nm (maximum power 30 mW).

Applications

Canopy height

Canopy height is an important variable needed to estimate the 3D properties of trees. Lidar-derived tree heights can be used to estimate various biophysical properties of trees based on allometric relationships between the biophysical properties and lidar-derived tree heights. In small-footprint scanning lidar systems with a pulse density of <1 pulse m^{-2}, underestimation of tree heights was a critical problem because the pulse density was insufficient to detect the

actual tree tops. Næsset (1997) reported that the mean tree height in coniferous stands derived from airborne lidar with a pulse density of 0.1 pulses m^{-2} was underestimated by 4.1–5.5 m compared with ground-measured data. In an attempt to solve this problem, Næsset divided forest stands into regular grids with cells of equal size and extracted only the maximum estimated height value within each cell. The lidar-derived mean height of stands was then computed as the arithmetic mean of these cell maxima. This method decreased the bias in mean tree height to <1.9 m. However, the area-based approach cannot satisfy the growing demand for feature extraction based on individual trees.

Small-footprint lidar systems with a high pulse density provide another solution for underestimation. The high pulse density increases the probability of laser hits on the actual tops of the trees and consequently reduces the magnitude of the underestimation. In a study by Maltamo *et al.* (2004*b*), tree heights of several species of Norway spruce (*Picea abies* L. Karst.), Scots pine (*Pinus sylvestris* L.), silver birch (*Betula pendula* Roth.), and downy birch (*Betula pubescens* Ehrh.) were estimated at a pulse density of 10 pulses m^{-2} (with a pulse repetition frequency of 83 kHz). The underestimation of tree height decreased to ~1 m. Omasa *et al*. (2000, 2003) used a lidar system with a pulse density of ~30 pulses m^{-2} to estimate tree height in Japanese coniferous and broadleaved forests. Their system increased the pulse density both by using a high pulse repetition frequency (25 kHz) and by using a helicopter with low flight speed as the scanning platform. This system allowed scanning of the entire ground surface, since the interval between neighbouring footprints was nearly equal to the footprint diameter. The accuracy of tree height measurement improved to <47 cm [with a root-mean-square error (RMSE) of 19 cm] for coniferous trees (five species) and 40 cm (RMSE=12 cm) for broadleaved trees (six species). These studies showed that the underestimation of tree height can be reduced by increasing the pulse density on the ground. The systems with a high pulse density not only reduced the underestimation of tree height but also allowed the production of high-resolution 3D images of each individual tree. Figure 2 shows 3D images of a woody canopy and of the terrain (ground surface) obtained by a helicopter-borne scanning lidar with a high pulse density (~30 pulses m^{-2}) (Omasa *et al*., 2000). The image processing process is illustrated in Fig. 1A. First- and last pulse-mode digital elevation models (FP-mode DEM, Fig. 2A; and LP-mode DEM, Fig. 2B) were produced from lidar data derived by first and last returned pulses, respectively. The digital terrain model (DTM, Fig. 2C) of a small valley was estimated with an accuracy of ~15 cm

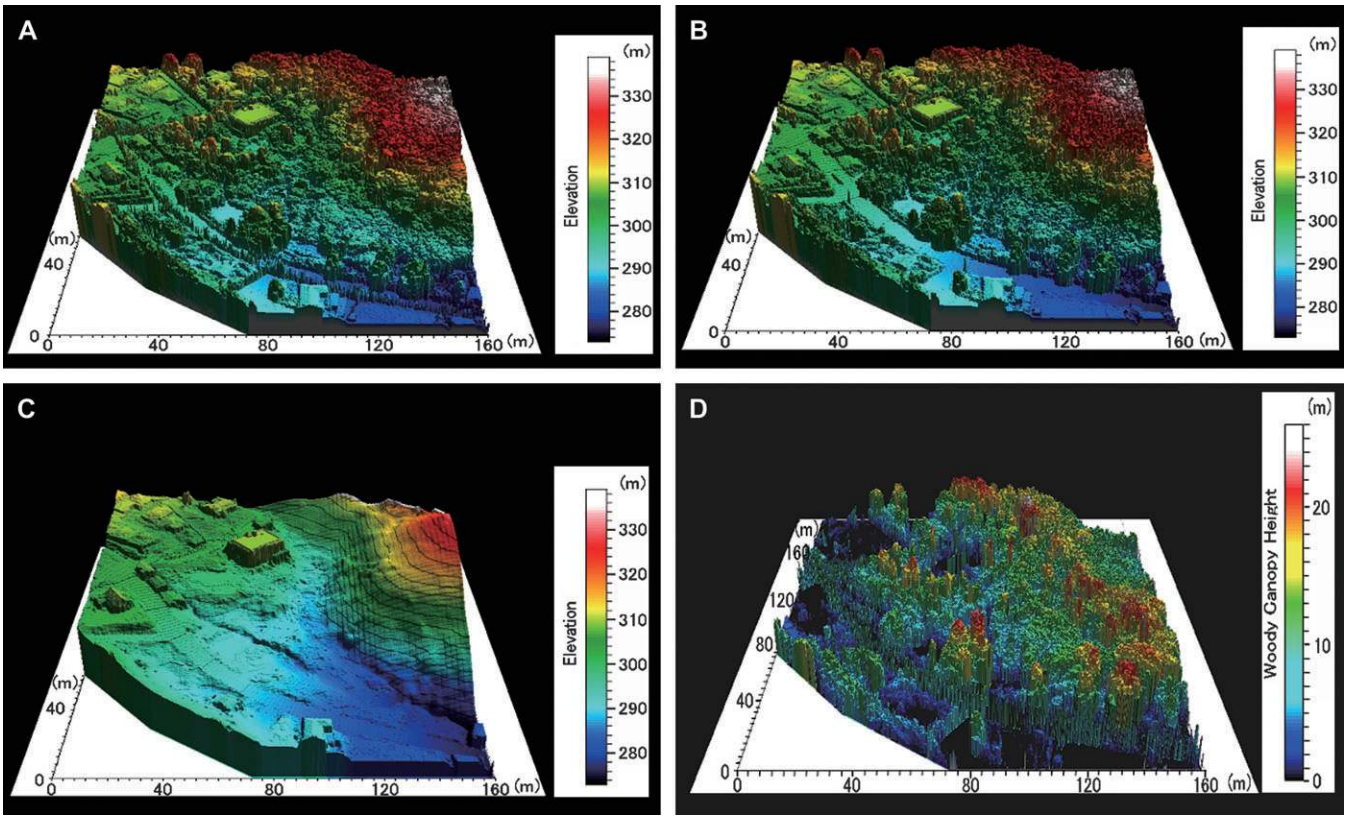

Fig. 2. 3D false-colour images (Omasa *et al*., 2000) of a small valley produced using high-resolution helicopter-borne small-footprint scanning lidar with a high pulse density (~30 pulses m^{-2}) and a 15 mm range accuracy. (A) FP-mode DEM. (B) LP-mode DEM. (C) DTM. (D) DCHM. In the images, coniferous and broadleaved trees, roads, houses, farmlands, streams, and other features can be seen.

by interpolating only LP-mode data reaching the ground surface. The net height of the woody canopy was calculated to produce a digital canopy-height model (DCHM, Fig. 2D) by subtracting the DTM elevations from the FP-mode DEM values.

An approach based on individual trees uses image-processing techniques to estimate the heights of individual trees together with tree position and crown area automatically. Several algorithms have been developed for this purpose, including the watershed algorithm (Hyyppä *et al*., 2001), the morphological computer vision method (Persson *et al*., 2002), the crown extraction filtering method (Omasa *et al*., 2003; details have not yet been published), and the local maximum method (Popescu *et al*., 2003; Popescu and Wynne, 2004). In some studies, basal area, stem volume, and stem density were regressed against lidar-derived individual tree heights and crown areas (Hyyppä *et al*., 2001; Persson *et al*., 2002; Omasa *et al*., 2003; Maltamo *et al*., 2004*a*). However, these algorithms can only be used with single-stemmed trees such as conifers.

Ground-based scanning lidar can provide more precise 3D images of individual trees with a typical resolution of 0.05–10 cm. 3D images generated from such systems provide much information about the trees, and each tree height can be estimated from the image, together with other variables (Omasa *et al*., 2002*b*; Urano and Omasa, 2003). The problem with operational measurements using ground-based lidar systems is that the laser beam may be unable to illuminate all the target trees because parts of some target trees may be hidden by other trees. To resolve this problem, target trees can be scanned from several measuring positions surrounding the target trees, and images acquired from these several points can be co-registered and merged, as shown in Fig. 1B (Hopkinson *et al*., 2004; Yoshimi *et al*., 2004; Hosoi *et al.*, 2005). The multiple images compensate for blind regions in some of the images, permitting accurate estimation of tree heights.

Canopy structure

Vegetation canopies play important roles in the interaction between plants and their environment through their effects on photosynthesis and transpiration. Therefore, changes in canopy structure can provide a sensitive indicator of responses to stress and adaptation of plants to their environment. However, it is still a challenge to measure canopy structure accurately due to its complex 3D structure. Recently, the ability of lidar to provide 3D data has been applied to the measurement of vertical foliage distribution, a key mensurational parameter used to represent the 3D canopy structure.

Magnussen and Boudewyn (1998) demonstrated that the distribution of canopy surface heights derived from a field trial of an airborne small-footprint lidar system in a Douglas-fir [*Pseudotsuga menziesii* (Mirb.) Franco] forest was related to the vertical distribution of foliage area. The vertical distribution of cumulative leaf area index (LAI) was estimated using the correlation between the height and foliage area distributions. In the study, the frequency of laser interception by the canopy was utilized as an index of foliage area at each height. In another study, gap probability was used instead of the frequency of interception (Lovell *et al*., 2003; Houldcroft *et al*., 2005). Gap probability is defined as the probability of non-interception of laser beams by the canopy. This probability was calculated at each height by tracing rays between points where the laser contacted the canopy and the lidar position. The probability was then related to LAI at each height using an exponential transformation on the assumption that foliage is randomly distributed throughout the canopy (Norman and Campbell, 1989; Welles and Norman, 1991). However, there have been some difficulties in accurately estimating the vertical foliage distribution using airborne small-footprint lidar systems. The vertical foliage profiles derived using such systems showed little response to the middle canopy levels that are present in actual foliage profiles because the systems can receive only the first and last returned pulses, and thus fail to record any reflections between the first and last returns (Lovell *et al*., 2003). Furthermore, non-uniformity in the leaf distribution, changes in beam angle, and the energy threshold of the returned pulse affect the accuracy of these estimates (Houldcroft *et al*., 2005). The presence of non-photosynthetic tissues (i.e. stem or branches) would also affect estimation accuracy.

The waveform-recording capability of airborne large-footprint lidar systems has been used to conduct canopy height profile (CHP) surveys, which represent the vertical distribution of canopy components. The CHP can be calculated by correcting for the effects of shading of upper foliage by lower foliage on the returned energy profile using an exponential transformation and the assumption of a uniform horizontal distribution of foliage (MacArthur and Horn, 1969; Lefsky *et al*., 1999*a*; Means *et al*., 1999). Although the CHP values are useful in estimating vertical canopy profiles over large scales, the accuracy of CHP is affected by non-uniformity of the horizontal distribution of actual foliage and the approach is thus less useful on smaller scales. In addition, the CHP does not represent the foliage height profile directly because of the effect of non-photosynthetic tissues within the canopy.

The optical point quadrat method is a method for roughly estimating vertical foliage profiles from the ground (MacArthur and Horn, 1969). The method is based on measuring heights to the lowest leaves above a set of sample points established on the ground beneath the canopy. A telephoto lens or clinometers with trigonometry was traditionally used to measure heights to the lowest leaves. A more modern version of this technique replaces these pieces of equipment with a non-scanning ground-based lidar system (Radtke and Bolstad, 2001; Parker *et al*., 2004).

Ground-based scanning lidar systems have also been applied to the gap probability method (Welles and Cohen, 1996; Lovell *et al*., 2003; Tanaka *et al*., 2004). A conventional method using gap probability is a popular technique for ground-based measurement of LAI, in which sunlight transmission beneath the canopy is measured by ceptometers (Norman and Campbell, 1989; Welles and Norman, 1991). Sunlight has been replaced by laser beams in the lidar equivalent of this technique. Studies based on the optical point quadrat and gap probability methods have improved the efficiency of data collection. However, it is still difficult for these methods to account for the effects of non-uniformity of the actual foliage distribution and the presence of non-photosynthetic tissue.

As described above, accurate estimation of the vertical foliage distribution is still difficult with either airborne or ground-based lidar systems. Recently, a voxel-based canopy profiling method (VCP method), in which the 3D space is divided into 'volume elements' (voxels) that are the 3D equivalent of the pixels in a two-dimensional (2D) image, has been developed for estimating vertical foliage profiles with reduced effects of any non-uniformity in the foliage distribution and of non-photosynthetic tissue (Hosoi and Omasa, 2006). An individual bambooleaf oak tree (*Quercus myrsinaefolia* Blume; LAI=4.9) was scanned from four measuring points during both the leaf-on and leaf-off using high-resolution ground-based scanning lidar, as shown in Fig. 3A (leaf-on) and 3B (leaf-off), respectively. The laser beam was able to illuminate the tree fully inside the canopy, as shown by the cross-sectional images presented in Fig. 4. By subtracting the leaf-off image from the leaf-on image, non-photosynthetic tissues can be eliminated from the data. The vertical foliage profile obtained in this manner was accurately estimated based on voxels estimated from the lidar-derived point-cloud data, and is shown in Fig. 5. The mean absolute percentage error, which was the arithmetic mean of the absolute percentage error between the actual and predicted (lidar-derived) value for each height, was 22%. The actual value of each height was measured by stratified clipping of the foliage. This method thus appears to be applicable for monitoring changes in canopy structure, although further improvement may be necessary and may be challenging to attain.

It has recently been demonstrated that species can be classified using 3D lidar data with a pulse density of 5.2–12 pulses m^{-2}. Brandtberg *et al.* (2003) scanned several leaf-off deciduous trees and extracted the vertical structure of the branches of each species using airborne small-footprint lidar. The absence of leaves in the canopy facilitated penetration by the laser beam in the deciduous forest so that the vertical structure of the branches could be more clearly extracted. Based on a lidar-derived height distribution and the proportion of laser return from the branches, the authors performed linear discriminant analysis on each individual tree for classification. Although the classification accuracy was only 60%, the potential of the lidar data to classify species was nonetheless apparent in this early work. Similarly, Holmgren and Persson (2004) demonstrated that airborne small-footprint lidar could distinguish between Norway spruce and Scots pine under leaf-on conditions. The lidar-derived variables used in this study were the proportion of laser returns, measurements of height distribution, canopy geometry, and intensity of returned pulses. Linear and quadratic discriminant analyses were performed on these lidar-derived variables for each individual tree. The results showed a 95% ability to distinguish between the two species correctly. Although these two studies focused on species classification, future works may allow this approach not only to classify species but also to estimate quantitatively the biophysical properties of each species.

Carbon stocks

Increases in atmospheric CO_2 concentration and climate changes vary the terrestrial carbon cycle and forest carbon stocks (Levy *et al*., 2004; Law, 2005; Shimizu *et al*., 2005).

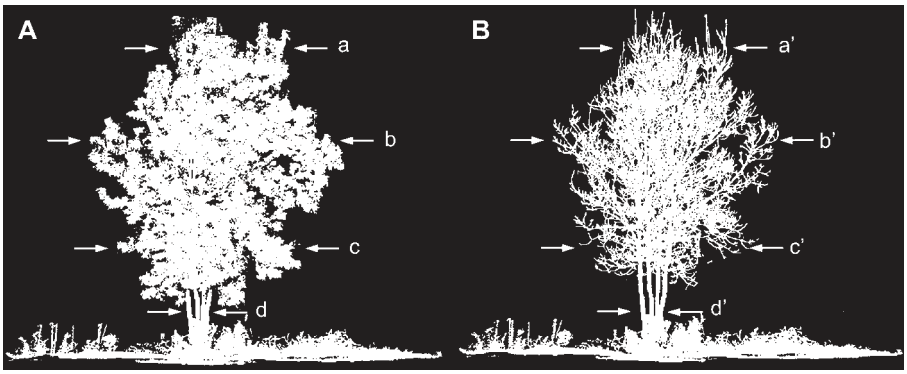

Fig. 3. 3D point-cloud images of an individual bambooleaf oak tree (*Quercus myrsinaefolia* Blume; LAI=4.9) growing in the field, obtained using high-resolution ground-based scanning lidar with an 8 mm range accuracy. (A) Leaf-on image. (B) Leaf-off image. Points a–d and a′–d′ represent the positions of the horizontal cross-sections displayed in Fig. 4.

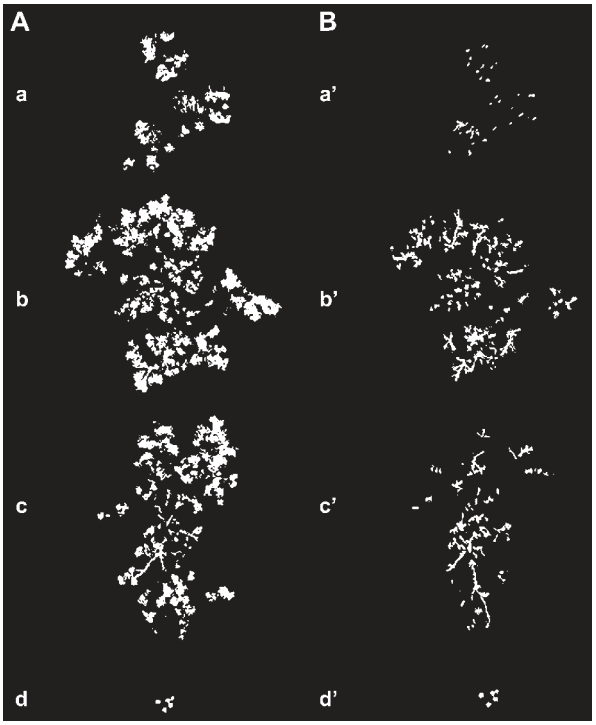

Fig. 4. Horizontal cross-sectional images of the bambooleaf oak tree (*Quercus myrsinaefolia* Blume) at each of the positions (a–d and a′–d′) shown in Fig. 3. (A) Leaf-on image. (B) Leaf-off image. These images show that lidar can obtain information within the canopy.

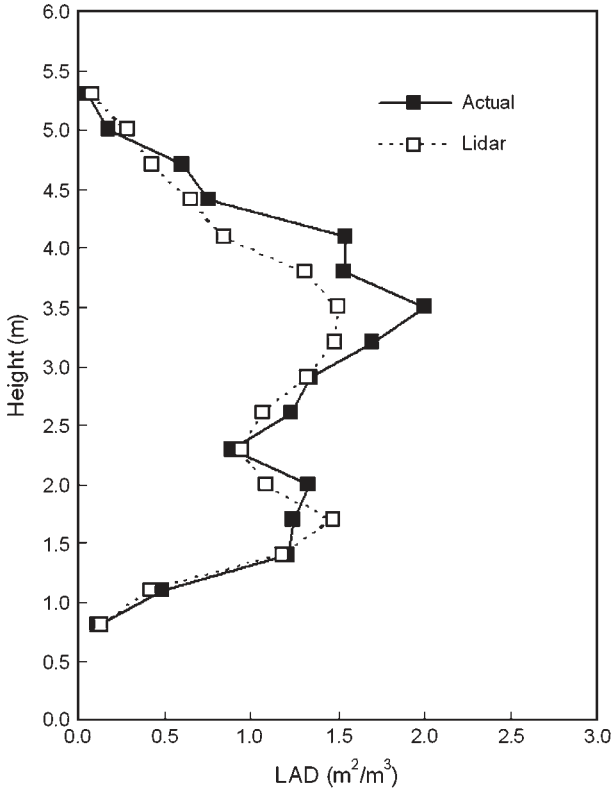

Fig. 5. Comparison between lidar-derived and actual profiles of leaf area density (LAD) of the bambooleaf oak tree (*Quercus myrsinaefolia* Blume) shown in Figs 3 and 4. The lidar-derived profile was estimated by means of a voxel-based canopy profiling method (Hosoi and Omasa, 2006); the actual profile was measured by stratified clipping of the foliage.

Accurate estimation of forest carbon stock capacity is requested by the Kyoto protocol to reduce greenhouse gases and global warming. It is also crucial for studying the functioning of forests and in studies of the terrestrial global carbon budget. In many cases, forest carbon stocks are estimated from limited site data, and the representativeness of such data is always uncertain because of the heterogeneity of forests. By contrast, remote sensing using passive optical systems or active radar sensors has allowed extraordinary advances in the modelling, mapping, and understanding of ecosystems over larger areas. However, these approaches have significant limitations in forestry applications because their sensitivity and accuracy have repeatedly been shown to decrease as above-ground biomass increases (Waring *et al*., 1995; Turner *et al*., 1999). Airborne and ground-based scanning lidar has provided novel alternatives for accurate and efficient large-scale estimation of forest carbon stocks.

Forest carbon stocks are defined as the amount of carbon per unit area (kg C m^{-2} or t C ha^{-1}), and also defined as the amount of carbon per tree (kg C $tree^{-1}$) for detailed representation of carbon stocks in each tree. Also, biomass can be converted into carbon stocks using a conversion factor based on the carbon content. Estimates of carbon stock can be regressed against lidar-derived variables. Total carbon stocks (stem, branches, foliage, and roots) of individual Japanese cedar [*Cryptomeria japonica* (L.f.) D. Don] trees could be mapped using a high-resolution DEM (Fig. 6) obtained using an airborne small-footprint lidar system with a high pulse density (~30 pulses m^{-1}), with the results shown in Fig. 7 (Omasa *et al*., 2003). Each tree height was estimated after segmentation of each tree canopy into individual trees. The carbon stock could then be estimated for each tree using allometric relationships between carbon stocks and lidar-derived tree height. The lidar-derived tree height has also been used for the estimation of carbon stocks in another study (Lim *et al*., 2003). For more heterogeneous forest, such as a forest with mixed species and ages, the distributions of lidar-derived canopy heights becomes a good indicator of the vertical canopy structure and can thus be used to estimate carbon stocks. Patenaude *et al.* (2004) estimated above-ground carbon stocks in mixed deciduous woodlands using the distributions of lidar-derived canopy heights rather than lidar-derived heights of dominant trees because the latter might not reflect the height distribution of a forest with mixed species and ages.

Means *et al*. (1999) and Lefsky *et al*. (1999*a*, *b*, 2002*a*) have also performed regressions of biomass against the canopy height derived using large-footprint lidar. Furthermore, data collected using such systems have been used

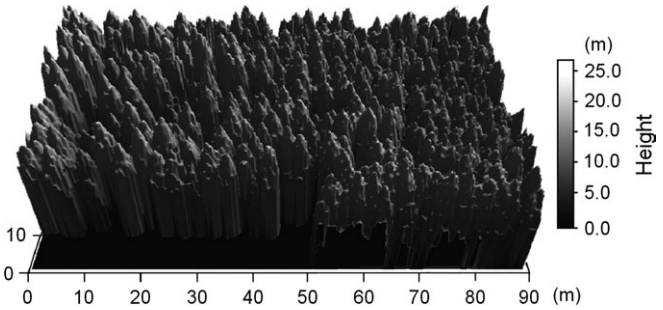

Fig. 6. 3D view of a DCHM obtained for a Japanese cedar (*Cryptomeria japonica* (L. f.) D. Don) forest using a helicopter-borne small-footprint scanning lidar system with 15 cm range accuracy (Omasa *et al*., 2003). The mesh of the DCHM was produced with a very high resolution (10 cm).

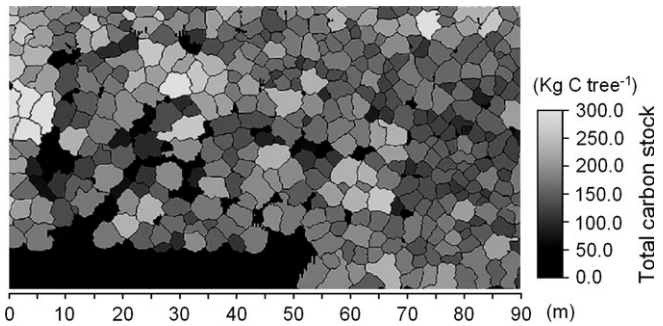

Fig. 7. Estimated total carbon stocks (stem, branches, foliage, and roots; kg C tree^{-1}) for each individual tree shown in Fig. 6 (Omasa *et al.*, 2003). Each polygon represents the total carbon stock of a single tree and covers the area occupied by the tree's canopy.

to estimate the gross primary production (GPP) and net primary production (NPP) of forests. The former is defined as the total amount of carbon that is fixed by plant photosynthesis in a certain period of time. The latter is defined as the net amount of primary production after the costs of plant respiration have been subtracted from GPP. GPP and NPP can be utilized as indicators of global plant responses. Kotchenova *et al.* (2004) used lidar-derived CHPs for a mixed-deciduous forest, calibrated using the total canopy field-measured LAIs, as input data for the vertical foliage distribution and coupled this distribution with models of GPP. They found that vertical foliage profiles were significantly correlated with GPP. The study also suggested that accounting for the actual vertical foliage profile can increase the accuracy of estimated daily GPP in photosynthesis models. Lefsky *et al.* (2005) used integrated lidar and Landsat data sets to characterize NPP over a spatially extensive set of plots in western Oregon. Stand age was mapped by means of iterative unsupervised classification of a multitemporal sequence of Landsat TM images (Cohen *et al*., 2002). NPP was then calculated as the average increment in lidar-estimated biomass during stand development. Both studies demonstrated the ability of lidar-based remote sensing to assess global-scale plant responses.

In ground-based scanning lidar systems, information on the underparts of trees becomes available. Based on this information, lidar-derived diameters at breast height (DBHs) can be used to estimate carbon stocks. Hopkinson *et al*. (2004) estimated the DBHs of trees in a red pine (*Pinus resinosa* Ait.) plantation and in a mixed deciduous stand dominated by sugar maple (*Acer saccharum* Marsh.) by selecting all lidar points between a height of 1.25 m and 1.75 m above the lowest point, then fitting a cylinder to the points. In this study, the authors measured the trees within a plot from several measuring points, thereby minimizing the number of blind regions (i.e. areas in which tree stems were obscured by other trees) and facilitating the extraction of DBH values. However, it is often difficult to scan all trees from several points in dense forest. Omasa *et al*. (2002*b*) scanned the stems in a Japanese larch (*Larix leptolepis* Gordon) forest with dense undergrowth (Fig. 8) from only one point, then estimated the stem diameter of each observable tree at a measurable height. The DBH of each tree was estimated accurately from the stem diameter at the measurable height using the relationship between stem diameter at specific height and DBH that was obtained from ground-truthing data. Although the DBHs of some trees within the surveyed area could not be estimated because of obstruction by dense undergrowth or other trees, this method nonetheless demonstrated the adaptability of ground-based lidar under difficult measuring conditions. Lidar-derived DBH can be converted into the carbon stock of each tree using allometric relationships between DBH and the carbon stock. The above-ground carbon stock of each larch tree in Fig. 8 was mapped (Fig. 9) and was correlated with the lidar-derived DBH (R^2=0.96), resulting in a 2.7% error in the average carbon stock (kg C m^{-2}) of larch trees within 30 m from the lidar position (Omasa *et al*., 2002*b*). Urano and Omasa (2003) applied this method to estimate the carbon stocks of stems, branches, leaves, and roots of Japanese cedars with an RMSE of 11.5 kg C tree^{-1} (total carbon stock=56.1–528.2 kg C tree^{-1}). The use of ground-based scanning lidar thus permits accurate and cost-effective estimation of individual tree carbon stock, and would therefore be applicable for the repeated measurements used in the studies of carbon stock monitoring.

Plant growth and shape changes

Plant growth is affected by various biotic stresses, such as diseases and insects, as well as by abiotic (environmental) stresses. Furthermore, global-scale plant growth has been shown to be affected by global climate change (Myneni *et al*., 1997; Menzel and Fabian, 1999; Andalo *et al*., 2005). Recently, plant growth at the forest-stand level has been monitored using airborne small-footprint lidar. Yu *et al.* (2004) measured individual trees between 1998 and 2000

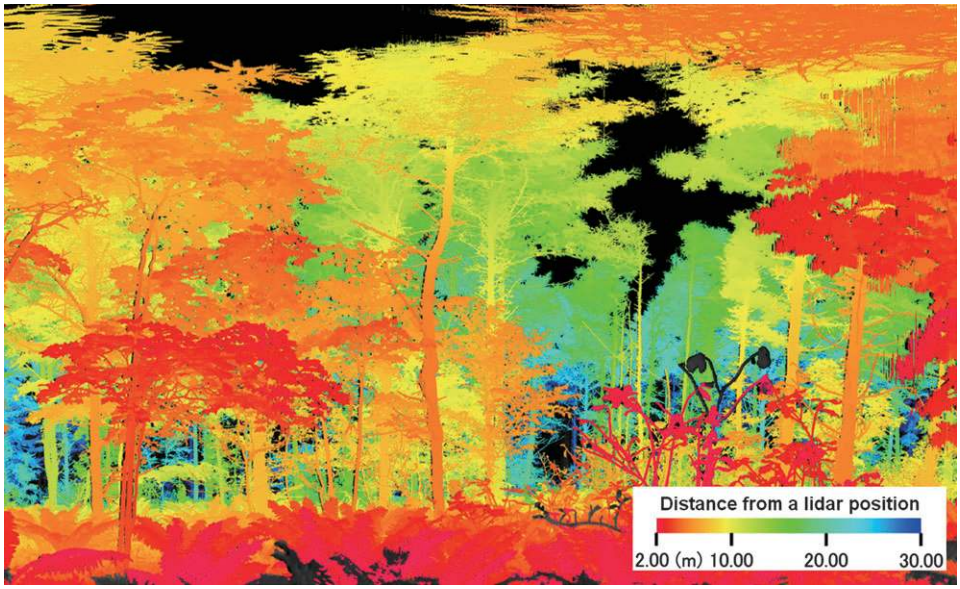

Fig. 8. False-colour image of a Japanese larch (*Larix leptolepis* Gordon) forest measured using a ground-based scanning lidar system with 8 mm range accuracy (Omasa *et al*., 2002*b*). Numerical values in the colour scale represent the distance from the lidar system.

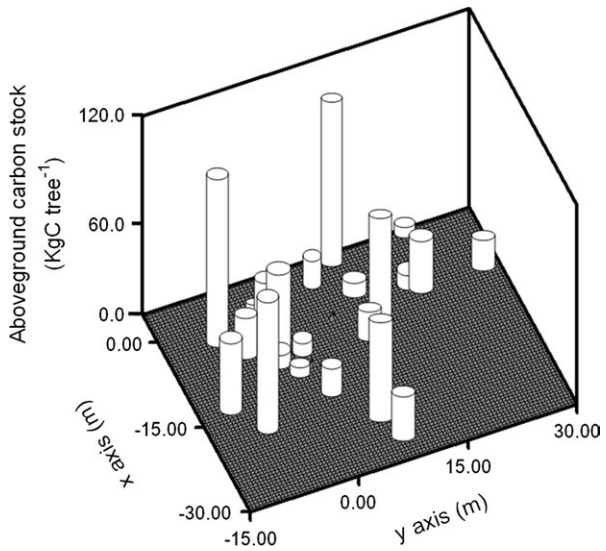

Fig. 9. Estimated above-ground carbon stock (kg C tree^{-1}) and stand position of each Japanese larch (*Larix leptolepis* Gordon) tree shown in Fig. 8. The *x*- and *y*-axes represent the horizontal plane in Fig. 8, and the origin represents the lidar position.

to monitor the growth of deciduous forests using small-footprint lidar with a sample density of 10 pulses m^{-2}. They developed a tree-to-tree matching algorithm to compare individual trees between survey dates. The growth of each tree was extracted by subtracting the tree height obtained in 1998 from the height measured in 2000 based on the matching results. The growth of the whole stand or in the individual plots ($\sim$25$\times$30 m^2) was obtained using the mean height difference for all matched trees. The accuracy of the estimated height growth was $\sim$5 cm at the stand level and $\sim$10–15 cm at the plot level. To monitor forest growth in a large area, Naesset and Gobakken (2005) used a small-footprint lidar system with a sampling density of 0.9–1.2 pulses m^{-2} in 1999 and 2001. Mean tree height, basal area, and stem volume were regressed against several lidar-derived variables (i.e. height percentiles, mean and maximum heights, coefficients of variation of the heights, and canopy density at different heights above the ground) based on the 1999 and 2001 lidar data. Forest growth was assumed to be solely responsible for the difference between the estimated biophysical variables in 2001 and 1999. Although the precision of the study was low, the study demonstrated the potential of this approach for monitoring plant growth over large areas.

Crops and vegetables grow much faster than forest trees, thus their growth rate becomes a sensitive and direct indicator of stress. Using high-precision ground-based scanning lidar, the growth of these plants can be depicted as a 3D shape change. Figure 10 shows an example of 3D growth monitoring for a small aubergine (*Solanum melongena* L.) seedling obtained using the above-mentioned optical probe-based scanning lidar, with a range accuracy of 0.5 mm at a distance of 3.5 m. Natural colour information was added to the images by means of a texture-mapping method (Heckbert, 1986; Haeberli and Segal, 1993; Soucy *et al.*, 1996; Omasa, 2000). As shown in Fig. 10, the lidar could clearly capture plant growth from 34 (Fig. 10A) to 52 d (Fig 10.C) after seeding by capturing the 3D expansion of leaves and stems and changes in the natural colour and texture of the plant elements.

Some stresses, such as water deficiency or severe heat, induce conformational responses in plants, such as leaf inclination, rolling, and wilting. Although 2D image analysis has been used for monitoring the responses to

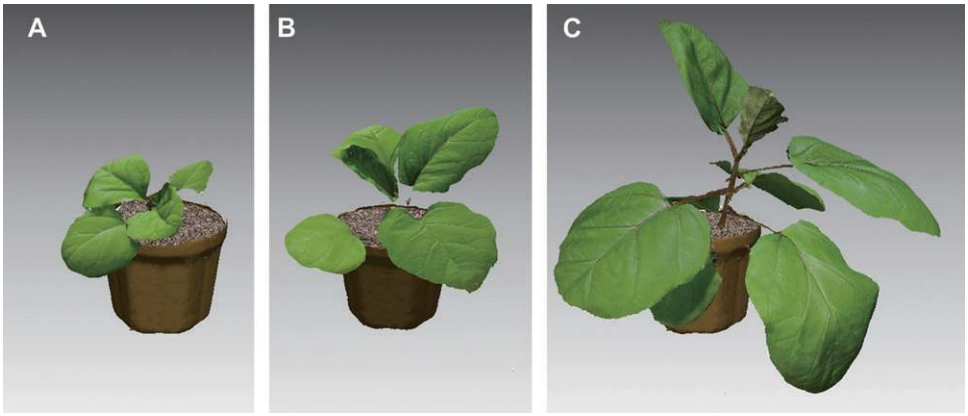

Fig. 10. Monitoring of aubergine (*Solanum melongena* L.) growth using high-resolution optical probe-based scanning lidar with a range accuracy of 0.5 mm at a distance of 3.5 m. Natural colour textural information was added to each lidar-derived image using a texture-mapping technique. A, B, and C are images of the aubergines at 34, 42, and 52 d after seeding, respectively. Growth conditions were 12 h of daylight with a photosynthetic photon flux density (PPFD) of 300 μmol m^{-2} s^{-1}, day/night temperatures and relative humidities of 26/22 °C and 40/60%, respectively.

such plant stresses (Kurata and Yan, 1996; Kacira *et al*., 2002; Foucher *et al*., 2004), it is difficult to monitor the shape responses fully solely by means of 2D imaging. Figure 11 shows an attempt at 3D monitoring of the shape response of a tomato (*Lycopersicum esculentum* Mill.) plant to water stress using the optical probe-based scanning lidar approach described above. The shape change (wilting) was clearly captured. The shape response to water stress is as sensitive an indicator as changes in stomatal response (Fujino *et al*., 2002).

Physiological responses and substances in leaves

Spectral analyses of reflection, radiation, and fluorescence from leaves have been widely used for imaging to detect photosynthesis, transpiration, stomatal response, and substances in the leaves (Omasa, 1990, 2002; Wessman, 1990; Omasa and Croxdale, 1992; Ustin *et al*., 1999; Buschmann *et al*., 2000; Govindjee and Nedbal, 2000; Kim *et al*., 2002; Omasa and Takayama 2002; Osmond and Park, 2002; Jones, 2004; Papageorgiou and Govindjee, 2004; Zarco-Tejada *et al*., 2004; Chaerle *et al*., 2005). Recent developments in this area of research are introduced in the Focus Papers in this issue. However, the majority of such research has been limited to 2D imaging. Mapping spectral images to an accurate 3D lidar image using computer graphics techniques such as texture mapping for natural colour images, as shown in Fig. 10, makes it possible to combine 3D images with biotic and physiological information. The composite image may provide more effective information for detecting and understanding 3D plant responses to stress.

For example, changes in 3D composite images of natural colour, chlorophyll *a* fluorescence intensity ('P' at the peak of the Kautsky effect), photochemical reflectance index (PRI), and leaf temperature of a sunflower (*Helianthus annuus* L.) plant in response to treatment with the herbicide glufosinate-ammonium (Basta) are shown in Figs 12 and 13. Basta is the most popular commercially available foliar herbicide used for weed control in many genetically engineered crops that have resistance to the herbicide (Lea and Ridley, 1989). Visible injury was not observed during the experiment. Natural colour is an indicator of the concentration of photosynthetic pigments such as

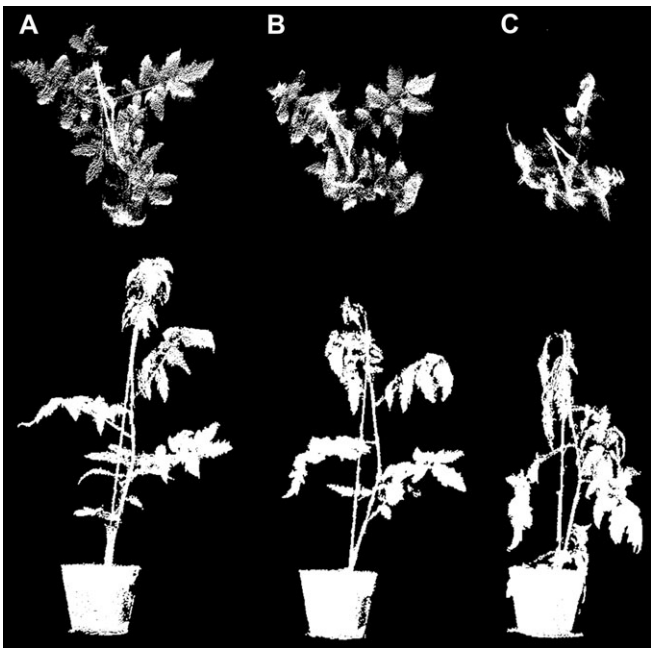

Fig. 11. Changes in the 3D shape of a tomato (*Lycopersicon esculentum* Mill.) plant in response to water stress obtained using optical probe-based scanning lidar with a 0.5 mm range accuracy. The upper and lower figures are top and side views, respectively. The water potentials of the plant in images A, B, and C were about −0.4, −0.7, and −1.5 MPa, respectively. The water deficit was caused by eliminating the water supply to the plant pot. Leaf inclination clearly changes as the water potential decreases. Growth conditions were the same as those described in Fig. 10.

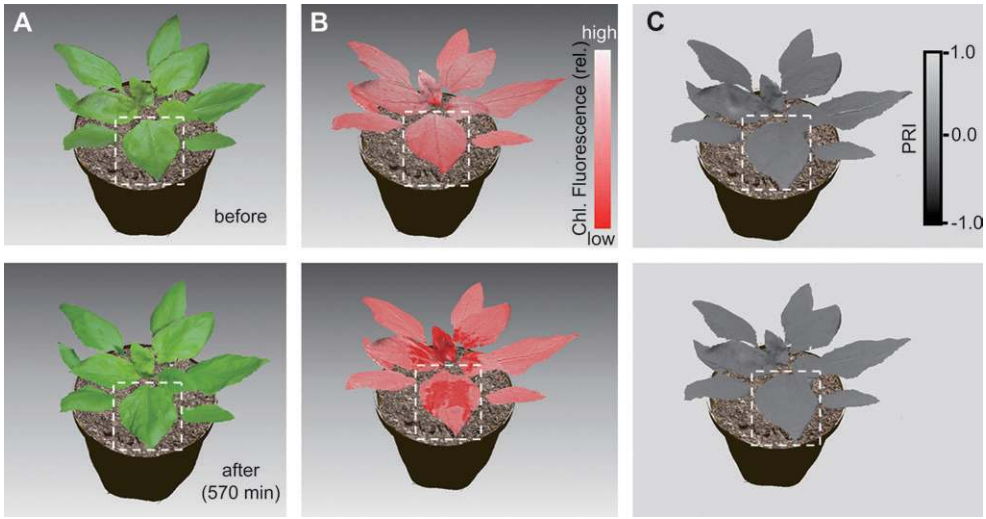

Fig. 12. Changes in 3D composite images of (A) the natural colour of a sunflower (*Helianthus annuus* L.) plant, (B) of chlorophyll (Chl.) *a* fluorescence intensity ('P' at the peak of the Kautsky effect), and (C) of the photochemical reflectance index (PRI) before (top row) and after (bottom row) treatment with glufosinate-ammonium (Basta) herbicide. The original 3D images were measured using an optical probe-based scanning lidar with 0.5 mm range accuracy. The composite images were obtained using a texture-mapping technique that mapped the natural colour, chlorophyll *a* fluorescence intensity, and PRI images to each 3D image. Broken lines show the part of the leaf to which the herbicide was applied. The upper images were measured ~180 min before the herbicide treatment and the lower ones were recorded ~570 min after the treatment. PPFD for fluorescence measurement (Omasa *et al*., 1987) was 250 μmol m^{-2} s^{-1}. Temperature and relative humidity were 25 °C and 50%, respectively. Growth conditions were the same as those described in Fig. 10.

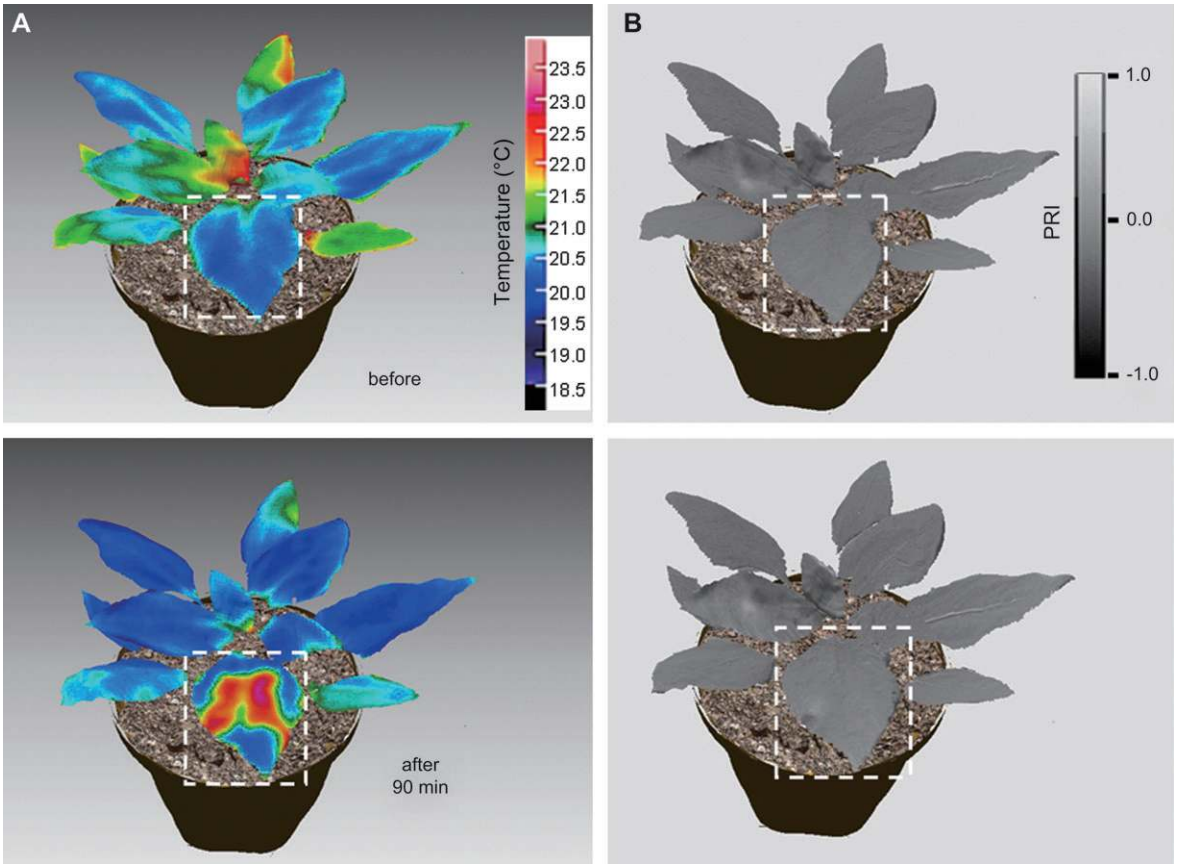

Fig. 13. Changes in 3D composite images of (A) leaf temperature and (B) PRI of the same plant shown in Fig. 12. The upper images were obtained just before the treatment and the lower ones were obtained 90 min after the treatment. Light was provided at a PPFD of 450 μmol m^{-2} s^{-1} from 180 min before the treatment, and stomata were mostly open by the time of the treatment. Temperature and relative humidity were 25 °C and 50%, respectively. Growth conditions were the same as those described in Fig. 10.

chlorophylls and carotenoids. Chlorophyll fluorescence, the first transient (OJIP) of a dark-adapted leaf, reflects the successive reduction of the electron acceptor pool in photosystem II (Q_A, the one-electron acceptor-bound plastoquinone; Q_B, the two-electron acceptor-bound plastoquinone; and mobile plastoquinone molecules), and 'P' may reflect the peak concentration of Q_A^-, Q_B^{2-}, and plastoquinone PQH_2 (Govindjee, 2004). PRI has a negative correlation with the de-epoxidation state of the xanthophyll cycle from violaxanthin to zeaxanthin (Gamon *et al*., 1992; Peñuelas *et al*., 1997; Evain *et al*., 2004) and it is calculated using the equation $(R_{531}–R_{570})/(R_{531}+R_{570})$, where R_k is the reflectance at a wavelength of k nm. Leaf temperature provides a measure of stomatal response, transpiration, absorption of CO_2 (photosynthesis), and absorption of air pollutants under constant thermal environments (Jones, 1983, 2004; Omasa, 1990, 2002).

Figure 12 represents 3D composite images of the natural colour, chlorophyll fluorescence intensity at 'P', and PRI before treatment with Basta on the central part of a leaf (broken lines in the figure) and at 570 min after the treatment. The active ingredient of Basta is glufosinate, which inhibits the activity of glutamine synthetase, which is essential for the removal of toxic ammonia produced by plant metabolism (Lea and Ridley, 1989). The application of glufosinate increases levels of ammonia in the plant tissues, and this reaction stops photosynthesis and causes mortality within a few days (Lea and Ridley, 1989). In Fig. 12, the natural colour and PRI images show little change, but a large change is evident in fluorescence intensity because of photosynthetic inhibition by 570 min after the treatment. Changes are also evident in other young leaves that had not been treated; the reason for these changes is not clear. Figure 13 shows 3D composite images of leaf temperature and PRI just before the treatment and 90 min after the treatment. Because illumination was provided starting at 180 min before the treatment, stomata had mostly opened before the treatment. The treatment caused stomatal closure and a temperature increase in the treated area. However, leaf temperature outside the treated area continued to decrease because of transpirational cooling permitted by the open stomata. As in Fig. 12, PRI at 90 min after the treatment showed little change from the pretreatment values. The difference in the spatial responses to Basta treatment was confirmed by simultaneous 3D imaging of natural colour, chlorophyll fluorescence, PRI, and leaf temperature.

Foliar chlorophyll contents are strongly related to the photosynthetic ability of plants. Leaf spectral reflectance is one means of assessing the contents of different chlorophylls. For example, chlorophyll *a* content was estimated (R^2=0.90) using the ratio of reflectance at 550 and 900 nm (Omasa and Aiga, 1987). The change in red edge, which is the region of the reflectance curve from 690 to 740 nm, also depends on the chlorophyll content (Curran *et al*., 1990; Jago *et al*., 1999). These analyses have been used to detect plant injuries that result from nutrient deficiency, air pollution, and other biotic and abiotic stresses that can cause changes in the chlorophyll content (Omasa and Aiga, 1987; Wessman, 1990; Ustin *et al*., 1999). Recent advances in hyperspectral imaging have provided additional useful information on physiological and ecophysiological reactions and on levels of various substances in plants (Wessman, 1990; Ustin *et al*., 1999; Zarco-Tejada *et al*., 2004). Thus, it may be possible to construct 3D composite images that include additional useful information by means of computer graphics. The spectral characteristics of plants have also been coupled with their 3D structure. Integrated analyses of spectral reflectance images and 3D lidar images provide more precise estimation of structural, physiological, and ecophysiological indices and levels of various substances in plants in wide-area imaging such as remote sensing. For example, Blackburn (2002) integrated an airborne multispectral sensor with an airborne small-footprint lidar system to estimate forest chlorophyll contents. Combining the 3D tree structure derived from the lidar image with the multispectral image improved the strength of the relationship between chlorophyll content per unit of leaf mass and the wavelength position of the red edge to R^2=0.85 for the coniferous stands.

Spectral analysis of steady-state fluorescence in the region between ultraviolet and red wavelengths (300–800 nm) has also been used for the detection of internal responses related to changes in plant pigments, cell structure, and membranes (Lang *et al.*, 1991; Lichtenthaler *et al.*, 1996; Buschmann *et al.*, 2000; Kim *et al*., 2002). Chlorophyll *a* fluorescence imaging, which was started by Omasa *et al.* (1987) and Daley *et al.* (1989), has been used as a powerful tool for non-invasive analysis of photosynthesis. The imaging reveals the distribution of photosynthetic activity within the leaf and permits early detection of stress before the appearance of visible injury on the leaf surface (Govindjee and Nedbal, 2000; Omasa and Takayama, 2002; Osmond and Park, 2002; Papageorgiou and Govindjee, 2004; Chaerle *et al*., 2005). Furthermore, because of the growing demand for large-scale monitoring of ecosystems in times of global change, the application of this form of imaging has been expanded from the leaf to whole plants and even forest stands. In particular, laser-induced fluorescence (LIF) imaging has been applied for the determination of substances in whole plants (Edner *et al*., 1994; Johansson *et al*., 1996; Saito *et al*., 2000) and photosynthetic activity of whole plants as techniques of laser-induced fluorescence transients (LIFTs) (Omasa, 1988, 1998; also see Omasa and Takayama, 2002; Kolber *et al*., 1998). Recently, more extensive characterization of photosynthetic properties, such as the efficiency of photosynthetic light utilization, the quantum yield of photosynthesis, and the kinetics of photosynthetic electron transport, has been proposed using LIFT, which is based on the

principles of fast-repetition fluorescence (Kolber *et al*., 1998) for large-scale measurement at a range of 5–30 m (Ananyev *et al*., 2005; Kolber *et al*., 2005).

Leaf temperature is a useful indicator of stomatal response, transpiration, and absorption of CO_2 (photosynthesis) and of air pollutants (Jones, 1983, 2004; Omasa, 1990, 2002; Omasa and Croxdale, 1992) under constant thermal conditions. In the early 1980s, Omasa *et al.* (1981*a*, *b*; also see Omasa and Croxdale, 1992) estimated dynamic responses in leaf images of stomatal resistance (i.e. the inverse of stomatal conductance), transpiration rate, and absorption rates of O_3, NO_2, and SO_2 from leaf-temperature images under a range of values of light intensity, air temperature, humidity, and air current. Recently, this technique was applied to simultaneous imaging of stomatal conductance, non-photochemical quenching, and photochemical yield of photosystem II in intact leaves (Omasa and Takayama, 2003). However, it is limited to imaging of a single leaf in a controlled environment. Chaerle *et al.* (2003) also applied thermal and chlorophyll fluorescence imaging for monitoring the effects of phenylurea herbicide on plant leaves. Further developments are presented in other Focus Papers in this issue.

Thermal imaging can permit the early detection of plant stress because stomatal closure occurs before the appearance of visible injury and this phenomenon is revealed by differences in temperature between stressed and non-stressed plants (Omasa, 1990, 2002; Jones, 2004). It is difficult to evaluate stomatal conductance and transpiration rates of plants under growing conditions in the field using leaf-temperature images because leaf temperature depends not only on stomatal opening but also on changeable thermal conditions such as air temperature, humidity, radiation, and air current. However, our previous studies have provided early detection of environmental stress in individual trees using ground-based or airborne (helicopter-based) thermal imaging under cloudy, slightly windy, and steady-state thermal conditions (Omasa and Aiga, 1987; Omasa *et al*., 1990, 1993; Omasa, 2002). Jones *et al*. (1997) and Jones (1999*a*, *b*) proposed a much more user-friendly approach based on the use of wet and dry reference surfaces to normalize the temperature of the leaf to account for changing environmental conditions and applied the technique to vegetation canopies in the field. Jones (2004) presents a detailed review of the application of thermal imaging and infrared sensing in plant physiology and ecophysiology.

Although fluorescence and thermal images provide useful information on plant stress, they are limited to 2D images. However, it is possible to create 3D images that will be more useful for detecting and understanding plant stress by compositing the 2D images with 3D lidar images, as shown in Figs 12 and 13. Furthermore, the use of 3D lidar images in mixel analysis in the 2D images (a mixel is a pixel whose value is a mixture of the different land cover radiance values) may improve the analytical results in wide-area imaging such as the spectral reflectance analysis described herein.

Concluding remarks and perspectives for the future

In this paper, a wide range of research on 3D lidar imaging from the leaf level to remote sensing of landscapes was reviewed. Numerous studies during the past decade have shown the applicability of lidar-based remote sensing to estimate plant properties such as canopy height, canopy structure, carbon stock, and species. Several studies have also demonstrated the usefulness of lidar in assessing large-scale plant growth responses. However, the potential of 3D lidar has not yet been fully exploited for monitoring of plant responses to stress. Future lidar applications, including more accurate dynamic estimation of plant properties, will improve our understanding of plant responses to stress and will improve our knowledge of interactions between plants and their environment.

The spectral properties of reflection, radiation, and fluorescence from leaves provide useful information on physiological responses and levels of various substances in leaves. However, until recently, most research on imaging these spectral properties has been limited to 2D imaging. Current passive imaging techniques such as multi- or hyperspectral imaging, thermal imaging, and active fluorescence imaging techniques can provide a variety of information on physiological conditions and levels of various substances in plants, including plant pigments, stomatal responses, transpiration, photosynthesis, and gas exchange. Therefore, the composite use of 3D lidar with 2D data collected using passive and active imaging techniques may improve the accuracy of airborne and satellite remote sensing and make it possible to analyse 3D information on physiological conditions and levels of various substances in agricultural and ecological applications and global biosphere observations.

To demonstrate the potential usefulness of composite imaging techniques, it was shown how accurate lidar images and optical images of natural colour, chlorophyll fluorescence, PRI, and leaf temperature can be combined to provide information on pigments, photosynthesis, transpiration, stomatal responses, and other factors at the level of individual plants using computer graphics techniques. The resulting 3D composite images will increasingly improve our understanding of and ability to diagnose plant responses to stress. Furthermore, the combination of lidar with other active imaging techniques is advantageous. In particular, the LIF and LIFT techniques are active forms of remote sensing that provide estimates of levels of various substances in leaves and of photosynthetic activity. Combination of these active imaging techniques with lidar may allow 3D estimates of levels

of various substances and of plant responses at multiple scales. In the future, composite 3D imaging techniques may be applied not only to plant science and global observations, but also to education, precision agriculture, and forestry.

References

Ananyev G, Kolber ZS, Klimov D, Falkowski PG, Berry JA, Rascher U, Martin R, Osmond B. 2005. Remote sensing of heterogeneity in photosynthetic efficiency, electron transport and dissipation of excess light in *Populus deltoides* stands under ambient and elevated CO_2 concentrations, and in a tropical forest canopy, using a new laser-induced fluorescence transient device. *Global Change Biology* **11,** 1195–1206.

Andalo C, Beaulieu J, Bousquet J. 2005. The impact of climate change on growth of local white spruce populations in Québec, Canada. *Forest Ecology and Management* **205,** 169–182.

Andersen HJ, Reng L, Kirk K. 2005. Geometric plant properties by relaxed stereo vision using simulated annealing. *Computers and Electronics in Agriculture* **49,** 219–232.

Askne JIH, Dammert PBG, Lars MH, Ulander LMH, Smith G. 1997. C-band repeat-pass interferometric SAR observations of the forest. *IEEE Transactions on Geoscience and Remote Sensing* **35,** 25–35.

Blackburn GA. 2002. Remote sensing of forest pigments using airborne imaging spectrometer and LIDAR imagery. *Remote Sensing of Environment* **82,** 311– 321.

Blair JB, Hofton MA. 1999. Modeling laser altimeter return waveforms over complex vegetation using high-resolution elevation data. *Geophysical Research Letters* **26,** 2509–2512.

Blair JB, Rabine DL, Hofton MA. 1999. The laser vegetation imaging sensor: a medium-altitude, digitisation-only, airborne laser altimeter for mapping vegetation and topography. *ISPRS Journal of Photogrammetry and Remote Sensing* **54,** 115–122.

Brandtberg T, Warner TA, Landenberger RE, McGraw JB. 2003. Detection and analysis of individual leaf-off tree crowns in small footprint, high sampling density lidar data from the eastern deciduous forest in North America. *Remote Sensing of Environment* **85,** 290–303.

Brooks MJ, de Agapito L, Huynh DQ, Baumela L. 1998. Towards robust metric reconstruction via a dynamic uncalibrated stereo head. *Image and Vision Computing* **16,** 989–1002.

Buschmann C, Langsdorf G, Lichtenthaler HK. 2000. Imaging of the blue, green, and red fluorescence emission of plants: an overview. *Photosynthetica* **38,** 483–491.

Chaerle L, Hulsen K, Hermans C, Strasser RJ, Valcke R, Hofte M, Van der Straeten D. 2003. Robotized time-lapse imaging to assess *in planta* uptake of phenylurea herbicides and their microbial degradation. *Physiologia Plantarum* **118,** 613–619.

Chaerle L, Saibo N, Van Der Straeten D. 2005. Tuning the pores: towards engineering plants for improved water use efficiency. *Trends in Biotechnology* **23,** 308–315.

Cohen WB, Spies TA, Alig RJ, Oetter DR, Maiersperger TK, Fiorella M. 2002. Characterizing 23 years (1972–95) of stand replacement disturbance in western Oregon forests with Landsat imagery. *Ecosystems* **5,** 122–137.

Curran PJ, Dungan JL, Gholz HL. 1990. Exploring the relationship between reflectance, red edge and chlorophyll content in slash pine. *Tree Physiology* **7,** 33–48.

Daley PF, Raschke K, Ball JT, Berry JA. 1989. Topography of photosynthetic activity of leaves obtained from video images of chlorophyll fluorescence. *Plant Physiology* **90,** 1233–1238.

Drake JB, Dubayah RO, Clark DB, Knox RG, Blair JB, Hofton MA, Chazdon RL, Weishampel JF, Prince SD. 2002. Estimation of tropical forest structural characteristics using large-footprint lidar. *Remote Sensing of Environment* **79,** 305–319.

Eckert S, Kellenberger T, Itten K. 2005. Accuracy assessment of automatically derived digital elevation models from aster data in mountainous terrain. *International Journal of Remote Sensing* **26,** 1943–1957.

Edner H, Johansson J, Svanberg S, Wallinder E. 1994. Fluorescence lidar multicolor imaging of vegetation. *Applied Optics* **33,** 2471–2479.

Evain S, Flexas J, Moya I. 2004. A new instrument for passive remote sensing. 2. Measurement of leaf and canopy reflectance changes at 531 nm and their relationship with photosynthesis and chlorophyll fluorescence. *Remote Sensing of Environment* **91,** 175–185

Flood M, Gutelius B. 1997. Commercial implications of topographic terrain mapping using scanning airborne laser radar. *Photogrammetric Engineering and Remote Sensing* **63,** 327–366.

Foucher P, Revollon P, Vigouroux B, Chassériaux G. 2004. Morphological image analysis for the detection of water stress in potted Forsythia. *Biosystems Engineering* **89,** 131–138.

Fujino M, Endo R, Omasa K. 2002. Nondestructive instrumentation of water-stressed cucumber leaves—comparison between changes in spectral reflectance, stomatal conductance and PSII yield and shape. *Agricultural Information Research* **11,** 161–170.

Gamon JA, Peñuelas J, Field CB. 1992. A narrow-waveband spectral index that tracks diurnal changes in photosynthetic efficiency. *Remote Sensing of Environment* **41,** 35–44.

Gong P, Mei XL, Biging GS, Zhang ZX. 2002. Improvement of an oak canopy model extracted from digital photogrammetry. *Photogrammetric Engineering and Remote Sensing* **68,** 919–924.

Govindjee, Nedbal L. 2000. Seeing is believing. *Photosynthetica* **38,** 481–482.

Govindjee. 2004. Chlorophyll *a* fluorescence: a bit of basics and history. In: Papageorgiou GC, Govindjee, eds. *Chlorophyll* a *fluorescence—a signature of photosynthesis*. Advances in Photosynthesis and Respiration, Vol. 19. New York: Springer, 1–41.

Häder DP. 1992. *Image analysis in biology.* Boca Raton, FL: CRC Press.

Häder DP. 2000. *Image analysis: methods and applications*, 2nd edn. Boca Raton, FL: CRC Press.

Haeberli P, Segal M. 1993. Texture mapping as a fundamental drawing primitive. In: *Proceedings of the Fourth Eurographics Workshop on Rendering.* Paris: Eurographics, 259–266.

Hagberg JO, Ulander LMH, Askne J. 1995. Repeat-pass SAR interferometry over forested terrain. *IEEE Transactions on Geoscience and Remote Sensing* **33,** 331–340.

Hashimoto Y, Kramer PJ, Nonami H, Strain BR. 1990. *Measurement techniques in plant science.* San Diego: Academic Press.

Hay CH, Warham J, Fineran BA. 2004. The vegetation of the Snares, islands south of New Zealand, mapped and discussed. *New Zealand Journal of Botany* **42,** 861–872.

He DX, Matsuura Y, Kozai T, Ting KC. 2003. A binocular stereovision system for transplant growth variables analysis. *Applied Engineering in Agriculture* **19,** 611–617.

Heckbert PS. 1986. Survey of texture mapping. *IEEE Computer Graphics and Applications* **6,** 56–67.

Hickman GD, Hogg JE. 1969. Application of an airborne pulsed laser for near shore bathymetric measurements. *Remote Sensing of Environment* **1,** 47–58.

Hobbs RJ, Mooney HA. 1990. *Remote sensing of biosphere functioning.* New York: Springer-Verlag.

Hoge FE, Swift RN, Frederick EB. 1980. Water depth measurement using an airborne pulsed neon laser system. *Applied Optics* **19,** 871–883.

Holmgren J, Persson Å. 2004. Identifying species of individual trees using airborne laser scanner. *Remote Sensing of Environment* **90,** 415–423.

Hopkinson C, Chasmer L, Young-Pow C, Treitz P. 2004. Assessing forest metrics with a ground-based scanning lidar. *Canadian Journal of Forest Research* **34,** 573–583.

Hosoi F, Omasa K. 2006. Voxel-based 3D modeling of individual trees for estimating leaf area density using high-resolution portable scanning lidar. *IEEE Transactions on Geoscience and Remote Sensing* (in press).

Hosoi F, Yoshimi K, Shimizu Y, Omasa K. 2005. 3-D measurement of trees using a portable scanning lidar. *Phyton* **45,** 497–500.

Houldcroft CJ, Campbell CL, Davenport IJ, Gurney RJ, Holden N. 2005. Measurement of canopy geometry characteristics using LiDAR laser altimetry: a feasibility study. *IEEE Transactions on Geoscience and Remote Sensing* **43,** 2270–2282.

Hyyppä J, Inkinen M. 1999. Detecting and estimating attributes for single trees using laser scanner. *Photogrammetric Journal of Finland* **16,** 27–42.

Hyyppä J, Kelle O, Lehikoinen M, Inkinen M. 2001. A segmentation-based method to retrieve stem volume estimates from 3-D tree height models produced by laser scanners. *IEEE Transactions on Geoscience and Remote Sensing* **39,** 969–975.

Ivanov N, Boissard P, Chapron M, Andrieu B. 1995. Computer stereo plotting for 3-D reconstruction of a maize canopy. *Agricultural and Forest Meteorology* **75,** 85–102.

Ivanov N, Boissard P, Chapron M, Valery P. 1994. Estimation of the height and angles of orientation of the upper leaves in the maize canopy using stereovision. *Agronomie* **14,** 183–194.

Jago RA, Cutler MEJ, Curran PJ. 1999. Estimating canopy chlorophyll concentration from field and airborne spectra. *Remote Sensing of Environment* **68,** 217–224.

Johansson J, Andersson M, Edner H, Mattsson J, Svanberg S. 1996. Remote fluorescence measurements of vegetation spectrally resolved and by multi-colour fluorescence imaging. *Journal of Plant Physiology* **148,** 632–637.

Jones HG. 1983. *Plants and microclimate.* Cambridge: Cambridge University Press.

Jones HG. 1999*a.* Use of thermography for quantitative studies of spatial and temporal variation of stomatal conductance over leaf surfaces. *Plant, Cell and Environment* **22,** 1043–1055.

Jones HG. 1999*b.* Use of infrared thermometry for estimation of stomatal conductance as a possible aid to irrigation scheduling. *Agricultural and Forest Meteorology* **95,** 139–149.

Jones HG. 2004. Application of thermal imaging and infrared sensing in plant physiology and ecophysiology. *Advances in Botanical Research* **41,** 107–163.

Jones HG, Aikman D, McBurney TA. 1997. Improvements to infrared thermometry for irrigation scheduling. *Acta Horticulturae* **449,** 259–266.

Kacira M, Ling PP, Short TH. 2002. Machine vision extracted plant movement for early detection of plant water stress. *Transactions of the ASAE* **45,** 1147–1153.

Kellndorfer J, Walker W, Pierce L, Dobson C, Fites JA, Hunsaker C, Vona J, Clutter M. 2004. Vegetation height estimation from shuttle radar topography mission and national elevation datasets. *Remote Sensing of Environment* **93,** 339–358.

Kim MS, Mulchi CL, McMurtrey JE, Daughtry CST, Chappele EM. 2002. Assessment of environmental plant stresses using multispectral steady-state fluorescence imagery. In: Omasa K, Saji H, Youssefian S, Kondo N, eds. *Air pollution and plant biotechnology.* Tokyo: Springer-Verlag, 321–341.

Kolber Z, Klimov D, Ananyev G, Rascher U, Berry J, Osmond B. 2005. Measuring photosynthetic parameters at a distance: laser induced fluorescence transient (LIFT) method for remote measurements of photosynthesis in terrestrial vegetation. *Photosynthesis Research* **84,** 121–129.

Kolber ZS, Prášil O, Falkowski PG. 1998. Measurements of variable chlorophyll fluorescence using fast repetition rate techniques: defining methodology and experimental protocols. *Biochimica et Biophysica Acta* **1367,** 88–106.

Kotchenova SY, Song X, Shabanov NV, Potter CS, Knyazikhin Y, Myneni RB. 2004. Lidar remote sensing for modeling gross primary production of deciduous forests. *Remote Sensing of Environment* **92,** 158–172.

Krabill WB, Collins JG, Link LE, Swift RN, Butler ML. 1984. Airborne laser topographic mapping results. *Photogrammetric Engineering and Remote Sensing* **50,** 685–694.

Kurata K, Yan J. 1996. Water stress estimation of tomato canopy based on machine vision. *Acta Horticulturae* **440,** 389–394.

Lang M, Stober F, Lichtenthaler HK. 1991. Fluorescence emission spectra of plant leaves and plant constituents. *Radiation and Environmental Biophysics* **30,** 333–347.

Law B. 2005. Carbon dynamics in response to climate and disturbance: recent progress from multi-scale measurements and modeling in AmeriFlux. In: Omasa K, Nouchi I, De Kok LJ, eds. *Plant responses to air pollution and global change.* Tokyo: Springer, 205–213.

Lea PJ, Ridley SM. 1989. Glutamine synthetase and its inhibition. In: Dodge AD, ed. *Herbicides and plant metabolism.* Cambridge: Cambridge University Press, 137–170.

Lefsky MA, Cohen WB, Acker SA, Parker GG, Spies TA, Harding D. 1999*a.* Lidar remote sensing of the canopy structure and biophysical properties of Douglas-fir western hemlock forests. *Remote Sensing of Environment* **70,** 339–361.

Lefsky MA, Cohen WB, Harding DJ, Parker GG, Acker SA, Gower ST. 2002*a.* Lidar remote sensing of above-ground biomass in three biomes. *Global Ecology and Biogeography* **11,** 393–399.

Lefsky MA, Cohen WB, Parker GG, Harding DJ. 2002*b.* Lidar remote sensing for ecosystem studies. *Bioscience* **52,** 19–30.

Lefsky MA, Harding D, Cohen WB, Parker G, Shugart HH. 1999*b.* Surface lidar remote sensing of basal area and biomass in deciduous forests of eastern Maryland, USA. *Remote Sensing of Environment* **67,** 83–98.

Lefsky MA, Turner DP, Guzy M, Cohen WB. 2005. Combining lidar estimates of above-ground biomass and Landsat estimates of stand age for spatially extensive validation of modeled forest productivity. *Remote Sensing of Environment* **95,** 549–558.

Levy PE, Cannell MGR, Friend AD. 2004. Modelling the impact of future changes in climate, CO_2 concentration and land use on natural ecosystems and the terrestrial carbon sink. *Global Environmental Change* **14,** 21–30.

Lichtenthaler HK, Lang M, Sowinska M, Heisel F, Miehe JA. 1996. Detection of vegetation stress via a new high resolution fluorescence imaging system. *Journal of Plant Physiology* **148,** 599–612.

Lim K, Treitz P, Baldwin K, Morrison I, Green J. 2003. Lidar remote sensing of biophysical properties of tolerant northern hardwood forests. *Canadian Journal of Remote Sensing* **29,** 658–678.

Liu CJ. 1995. Using portable laser EDM for forest traverse surveys. *Canadian Journal of Forest Research* **25,** 753–766.

Lovell JL, Jupp DLB, Culvenor DS, Coops NC. 2003. Using airborne and ground-based ranging lidar to measure canopy structure in Australian forests. *Canadian Journal of Remote Sensing* **29,** 607–622.

MacArthur RH, Horn HS. 1969. Foliage profile by vertical measurements. *Ecology* **50,** 802–804.

Maclean GA, Krabill WB. 1986. Gross-merchantable timber volume estimation using an airborne lidar system. *Canadian Journal of Remote Sensing* **12,** 7–18.

Magnussen S, Boudewyn P. 1998. Derivations of stand heights from airborne laser scanner data with canopy-based quantile estimators. *Canadian Journal of Forest Research* **28,** 1016–1031.

Maltamo M, Eerikäinen K, Pitkänen J, Hyyppä J, Vehmas M. 2004*a.* Estimation of timber volume and stem density based on scanning laser altimetry and expected tree size distribution functions. *Remote Sensing of Environment* **90,** 319–330.

Maltamo M, Mustonen K, Hyyppä J, Pitkänen J, Yu X. 2004*b.* The accuracy of estimating individual tree variables with airborne laser scanning in a boreal nature reserve. *Canadian Journal of Forest Research* **34,** 1791–1801.

Mayers VI. 1983. Remote sensing applications in agriculture. In: Colwell RN, ed. *Manual of remote sensing*, 2nd edn. Vol. II. Falls Church, VA: American Society of Photogrammetry and Remote Sensing.

Means JE, Acker SA, Harding DJ, Blair JB, Lefsky MA, Cohen WB, Harmon ME, McKee WA. 1999. Use of large-footprint scanning airborne lidar to estimate forest stand characteristics in the Western Cascades of Oregon. *Remote Sensing of Environment* **67,** 298–308.

Menzel A, Fabian P. 1999. Growing season extended in Europe. *Nature* **397,** 659.

Myneni RB, Keeling CD, Tucker CJ, Asrar G, Nemani RR. 1997. Increased plant growth in the northern high latitudes from 1981 to 1991. *Nature* **386,** 698–702.

Næsset E. 1997. Determination of mean tree height of forest stands using airborne laser scanner data. *ISPRS Journal of Photogrammetry and Remote Sensing* **52,** 49–56.

Næsset E, Gobakken T. 2005. Estimating forest growth using canopy metrics derived from airborne laser scanner data. *Remote Sensing of Environment* **96,** 453–465.

Næsset E, Gobakken T, Holmgren J, Hyyppä H, Hyyppä J, Maltamo M, Nilsson M, Olsson H, Persson Å, Söderman U. 2004. Laser scanning of forest resources: the Nordic experience. *Scandinavian Journal of Forest Research* **19,** 482–499.

Negahdaripour S, Hayashi BY, Aloimonos Y. 1995. Direct motion stereo for passive navigation. *IEEE Transactions on Robotics and Automation* **11,** 829–843.

Nelson R, Krabill W, Maclean G. 1984. Determining forest canopy characteristics using airborne laser data. *Remote Sensing of Environment* **15,** 201–212.

Nelson R, Krabill W, Tonelli J. 1988. Estimating forest biomass and volume using airborne laser data. *Remote Sensing of Environment* **24,** 247–267.

Norman JM, Campbell GS. 1989. Canopy structure. In: Pearcy RW, Ehleringer J, Mooney HA, Rundel PW, eds. *Plant physiological ecology: field methods and instrumentation.* London: Chapman and Hall, 301–326.

Omasa K. 1988. Image instrumentation of plants using a laser scanner. In: *Proceeding of Annual Meeting of Japanese Society of Environment Control in Biology.* Utsunomiya: Japanese Society of Environment Control in Biology, 14–15.

Omasa K. 1990. Image instrumentation methods of plant analysis. In: Linskens HF, Jackson JF, eds. *Modern methods of plant analysis.* Berlin: Springer-Verlag, 203–243.

Omasa K. 1998. Image instrumentation of chlorophyll *a* fluorescence. *Proceedings of the International Society for Optical Engineering (SPIE)* **3382,** 91–99.

Omasa K. 2000. 3-D color video microscopy. In: Häder DP, ed. *Image analysis: methods and applications*, 2nd edn. Boca Raton, FL: CRC Press, 257–273.

Omasa K. 2002. Diagnosis of stomatal response and gas exchange of trees by thermal remote sensing. In: Omasa K, Saji H, Youssefian S, Kondo N, eds. *Air pollution and plant biotechnology.* Tokyo: Springer-Verlag, 343–359.

Omasa K. 2006. Image sensing and phytobiological information. In: *CIGR handbook of agricultural engineering*, Vol. 6. MI: ASABE.

Omasa K, Aiga I. 1987. Environmental measurement: image instrumentation for evaluating pollution effects on plants. In: Singh MG, ed. *Systems and control encyclopedia.* Oxford: Pergamon Press, 1516–1522.

Omasa K, Akiyama Y, Ishigami Y, Yoshimi K. 2000. 3-D remote sensing of woody canopy heights using a scanning helicopter-borne lidar system with high spatial resolution. *Journal of Remote Sensing Society of Japan* **20,** 394–406.

Omasa K, Croxdale JG. 1992. Image analysis of stomatal movements and gas exchange. In: Häder DP, ed. *Image analysis in biology.* Boca Raton, FL: CRC Press, 171–197.

Omasa K, Hashimoto Y, Aiga I. 1981*a.* A quantitative analysis of relationships between SO_2 or NO_2 sorption and their acute effects on plant leaves using image instrumentation. *Environmental Control in Biology* **19,** 59–67.

Omasa K, Hashimoto Y, Aiga I. 1981*b.* A quantitative analysis of the relationships between O_3 sorption and its acute effects on plant leaves using image instrumentation. *Environmental Control in Biology* **19,** 85–92.

Omasa K, Nouchi I, De Kok LJ. 2005. *Plant responses to air pollution and global change.* Tokyo: Springer-Verlag.

Omasa K, Oki K, Suhama T. 2006. Remote sensing from satellite and aircraft. In: *CIGR Handbook of Agricultural Engineering*, Vol. 6. MI: ASABE.

Omasa K, Qiu GY, Watanuki K, Yoshimi K, Akiyama Y. 2003. Accurate estimation of forest carbon stocks by 3-D remote sensing of individual trees. *Environmental Science and Technology* **37,** 1198–1201.

Omasa K, Saji H, Youssefian S, Kondo N. 2002*a. Air pollution and plant biotechnology.* Tokyo: Springer-Verlag.

Omasa K, Shimazaki K, Aiga I, Larcher W, Onoe M. 1987. Image analysis of chlorophyll fluorescence transients for diagnosing the photosynthetic system of attached leaves. *Plant Physiology* **84,** 748–752.

Omasa K, Shimizu H, Ogawa K, Matsuki A. 1993. Diagnosis of trees from helicopter by thermographic system. *Environmental Control in Biology* **31,** 161–168.

Omasa K, Tajima A, Miyasaka K. 1990. Diagnosis of street trees by thermography: Zelkoba trees in Sendai city. *Journal of Agricultural Meteorology* **45,** 271–275.

Omasa K, Takayama K. 2002. Image instrumentation of chlorophyll *a* fluorescence for diagnosing photosynthetic injury. In: Omasa K, Saji H, Youssefian S, Kondo N, eds. *Air pollution and plant biotechnology.* Tokyo: Springer-Verlag, 287–308.

Omasa K, Takayama K. 2003. Simultaneous measurement of stomatal conductance, non-photochemical quenching, and photochemical yield of photosystem II in intact leaves by thermal and chlorophyll fluorescence imaging. *Plant and Cell Physiology* **44,** 1290–1300.

Omasa K, Urano Y, Oguma H, Fujinuma Y. 2002*b.* Mapping of tree position of *Larix leptolepis* woods and estimation of diameter at breast height (DBH) and biomass of the trees using range data measured by a portable scanning lidar. *Journal of Remote Sensing Society of Japan* **22,** 550–557.

Osmond B, Park YM. 2002. Field-portable imaging system for measurement of chlorophyll fluorescence quenching. In: Omasa K, Saji H, Youssefian S, Kondo N, eds. *Air pollution and plant biotechnology.* Tokyo: Springer-Verlag, 309–319.

Oxborough K. 2004. Using chlorophyll *a* fluorescence imaging to monitor photosynthetic performance. In: Papageorgiou GC, Govindjee, eds. *Chlorophyll* a *fluorescence—a signature of photosynthesis. Advances in Photosynthesis and Respiration*, Vol. 19. New York: Springer, 409–428.

Papageorgiou GC, Govindjee (eds). 2004. *Chlorophyll* a *fluorescence—a signature of photosynthesis. Advances in Photosynthesis and Respiration*, Vol. 19. New York: Springer.

Papathanassiou KP, Cloude SR. 2001. Single-baseline polarimetric SAR interferometry. *IEEE Transactions on Geoscience and Remote Sensing* **39,** 2352–2363.

Parker GG, Harding DJ, Berger ML. 2004. A portable LIDAR system for rapid determination of forest canopy structure. *Journal of Applied Ecology* **41,** 755–767.

Patenaude G, Hill RA, Milne R, Gaveau DLA, Briggs BBJ, Dawson TP. 2004. Quantifying forest above-ground carbon content using LiDAR remote sensing. *Remote Sensing of Environment* **93,** 368–380.

Peet FG, Morrison DJ, Pellow KW. 1997. Using a hand-held electronic laser-based survey instrument for stem mapping. *Canadian Journal of Forest Research* **27,** 2104–2108.

Peñuelas J, Llusia J, Piñol J, Filella I. 1997. Photochemical reflectance index and leaf photosynthetic radiation-use-efficiency assessment in Mediterranean trees. *International Journal of Remote Sensing* **18,** 2863–2868.

Persson Å, Holmgren J, Söderman U. 2002. Detecting and measuring individual trees using an airborne laser scanner. *Photogrammetric Engineering and Remote Sensing* **68,** 925–932.

Popescu SC, Wynne RH. 2004. Seeing the trees in the forest: using lidar and multispectral data fusion with local filtering and variable window size for estimating tree height. *Photogrammetric Engineering and Remote Sensing* **70,** 589–604.

Popescu SC, Wynne RH, Nelson RF. 2003. Measuring individual tree crown diameter with lidar and assessing its influence on estimating forest volume and biomass. *Canadian Journal of Remote Sensing* **29,** 564–577.

Radtke PJ, Bolstad PV. 2001. Laser point-quadrat sampling for estimating foliage-height profiles in broad-leaved forests. *Canadian Journal of Forest Research* **31,** 410–418.

Reutebuch SE, Andersen HE, McGaughey RJ. 2005. Light detection and ranging (LIDAR): an emerging tool for multiple resource inventory. *Journal of Forestry* **103,** 286–292.

Saito Y, Saito R, Kawahara TD, Nomura A, Takeda S. 2000. Development and performance characteristics of laser-induced fluorescence imaging lidar for forestry applications. *Forest Ecology and Management* **128,** 129–137.

Schreier H, Lougheed J, Gibson JR, Russell J. 1984. Calibrating an airborne laser profiling system. *Photogrammetric Engineering and Remote Sensing* **50,** 1591–1598.

Schurr U, Walter A, Rascher U. 2006. Functional dynamics of plant growth and photosynthesis—from steady-state to dynamics—from homogeneity to heterogeneity. *Plant, Cell and Environment* **29,** 340–352.

Schurr U, Walter A, Terjung S, Spies H, Kirchgessner N, Scharr H, Küsters R. 2001. Dynamics of leaf and root growth. In: *Proceedings of the 12th International Congress on Photosynthesis.* Melbourne: CSIRO Publishing.

Sheng YW, Gong P, Biging GS. 2001. Model-based conifer-crown surface reconstruction from high-resolution aerial images. *Photogrammetric Engineering and Remote Sensing* **67,** 957–965.

Shimizu Y, Hajima T, Omasa K. 2005. Assessments of climate change impacts on the terrestrial ecosystem in Japan using the BioGeographical and GeoChemical (BGGC) model. In: Omasa K, Nouchi I, De Kok LJ, eds. *Plant responses to air pollution and global change.* Tokyo: Springer-Verlag, 235–240.

Shirai Y. 1972. Recognition of polyhedrons with a range finder. *Pattern Recognition* **4,** 243–250.

Soucy M, Godin G, Rioux M. 1996. A texture-mapping approach for the compression of colored 3D triangulations. *The Visual Computer* **12,** 503–514.

Tanaka T, Park H, Hattori S. 2004. Measurement of forest canopy structure by a laser plane range-finding method improvement of radiative resolution and examples of its application. *Agricultural and Forest Meteorology* **125,** 129–142.

Toutin T. 2004. Comparison of stereo-extracted DTM from different high-resolution sensors: SPOT-5, EROS-A, IKONOS-II, and QuickBird. *IEEE Transactions on Geoscience and Remote Sensing* **42,** 2121–2129.

Turner DP, Cohen WB, Kennedy RE, Fassnacht KS, Briggs JM. 1999. Relationships between leaf area index and Landsat TM spectral vegetation indices across three temperate zone sites. *Remote Sensing of Environment* **70,** 52–68.

Urano Y, Omasa K. 2003. Accurate estimation of forest stand parameters in Japanese cedar woods using a portable scanning lidar. In: *Proceedings of IAWPS2003.* Daejeon, Korea, 403–407.

Ustin SL, Smith MO, Jacquemound S, Verstraete M, Govaerts Y. 1999. Geobotany: vegetation mapping for earth sciences. In: Rencz AN, ed. *Remote sensing for the earth sciences: manual of remote sensing*, 3rd edn. Vol. 3. New York: John Wiley & Sons, 189–248.

Vanderbilt VC. 1985. Measuring plant canopy structure. *Remote Sensing of Environment* **18,** 281–294.

Waring RH, Way JB, Hunt ER, Morrissey L, Ranson KJ, Weishampel JF, Oren R, Franklin SE. 1995. Biologists toolbox—imaging radar for ecosystem studies. *Bioscience* **45,** 715– 723.

Welles JM, Cohen S. 1996. Canopy structure measurement by gap fraction analysis using commercial instrumentation. *Journal of Experimental Botany* **47,** 1335–1342.

Welles JM, Norman JM. 1991. Instrument for indirect measurement of canopy architecture. *Agronomy Journal* **83,** 818–825.

Wessman CA. 1990. Evaluation of canopy biochemistry. In: Hobbs RJ, Mooney HA, eds. *Remote sensing of biosphere functioning.* New York: Springer-Verlag, 135–156.

Williams MS, Cormier KL, Briggs RG, Martinez DL. 1999. Evaluation of the Barr & Stroud FP15 and Criterion 400 laser dendrometers for measuring upper stem diameters and heights. *Forest Science* **45,** 53–61.

Yoshimi K, Hosoi F, Shimizu Y, Yamada H, Omasa K. 2004. 3D measurement of terrain and woody canopy height using portable scanning lidar. *Eco-Engineering* **16,** 203–207.

Yu X, Hyyppä J, Kaartinen H, Maltamo M. 2004. Automatic detection of harvested trees and determination of forest growth using airborne laser scanning. *Remote Sensing of Environment* **90,** 451–462.

Zarco-Tejada PJ, Berjón A, Miller JR. 2004. Stress detection in crops with hyperspectral remote sensing and physical simulation models. In: *Proceedings of Airborne Imaging Spectroscopy Workshop.* Bruges, Belgium: Belgian Federal Science Policy.

Zomer R, Ustin S, Ives J. 2002. Using satellite remote sensing for DEM extraction in complex mountainous terrain: landscape analysis of the Makalu Barun National Park of eastern Nepal. *International Journal of Remote Sensing* **23,** 125–143.